

1 **RESEARCH ARTICLE**

2
3 **SMC5/6 complex-mediated SUMOylation stimulates DNA-protein crosslink**
4 **repair in Arabidopsis**

5
6 Eva Dvořák Tomašítková^{a,3}, Klara Prochazkova^a, Fen Yang^{a,b}, Jitka Jemelkova^{a,c}, Andreas
7 Finke^{d,2}, Annika Dorn^e, Mahmoud Said^{a,f}, Holger Puchta^e, Ales Pecinka^{a,b,c,3}

8
9 ^aCentre of Plant Structural and Functional Genomics, Institute of Experimental Botany (IEB),
10 Czech Acad Sci, Šlechtitelů 31, 77900 Olomouc, Czech Republic.

11 ^bDepartment of Cell Biology and Genetics, Faculty of Science, Palacký University, Olomouc,
12 Czech Republic.

13 ^cFunctional Genomics and Proteomics, National Centre for Biomolecular Research (NCBR),
14 Faculty of Science, Masaryk University, Kamenice 5, 62500 Brno, Czech Republic.

15 ^dMax Planck Institute for Plant Breeding Research, Carl-von-Linné-Weg 10, 50829 Cologne,
16 Germany.

17 ^eBotanical Institute, Molecular Biology and Biochemistry, Karlsruhe Institute of Technology,
18 Fritz-Haber-Weg 4, Karlsruhe, 76131, Germany.

19 ^fField Crops Research Institute, Agricultural Research Centre, 9 Gamma Street, Giza, 12619,
20 Cairo, Egypt.

21
22 ²Present address: Hamilton Bonaduz AG, Application Laboratory, CH-4123 Allschwil,
23 Switzerland.

24
25 **Short title:** DPC repair by SMC5/6 complex

26
27
28
29 The author(s) responsible for distribution of materials integral to the findings presented in this
30 article, in accordance with the policy described in the Instructions for Authors
31 (<https://academic.oup.com/plcell/>) is: Ales Pecinka (pecinka@ueb.cas.cz).

32
33 ³Corresponding authors: Ales Pecinka (pecinka@ueb.cas.cz), Eva Dvořák Tomašítková
34 (tomastikova@ueb.cas.cz)

35
36 **Keywords:** SMC5/6 complex, SUMO, DNA damage repair, DNA-protein crosslink, WSS1,
37 genome stability

38

39 **ABSTRACT**

40 DNA-protein crosslinks (DPCs) are highly toxic DNA lesions consisting of proteins covalently
41 attached to chromosomal DNA. Unrepaired DPCs physically block DNA replication and
42 transcription. Three DPC repair pathways have been identified in *Arabidopsis* (*Arabidopsis*
43 *thaliana*) to date: the endonucleolytic cleavage of DNA by the structure-specific
44 endonuclease MUS81; proteolytic degradation of the crosslinked protein by the
45 metalloprotease WSS1A; and cleavage of the crosslink phosphodiester bonds by the tyrosyl
46 phosphodiesterases TDP1 and TDP2. Here we describe the evolutionary conserved
47 STRUCTURAL MAINTENANCE OF CHROMOSOMES SMC5/6 complex as a crucial
48 component involved in DPC repair. We identified multiple alleles of the SMC5/6 complex
49 core subunit gene *SMC6B* via a forward-directed genetic screen designed to identify the
50 factors involved in the repair of DPCs induced by the cytidine analog zebularine. We
51 monitored plant growth and cell death in response to DPC-inducing chemicals, which
52 revealed that the SMC5/6 complex is essential for the repair of several types of DPCs.
53 Genetic interaction and sensitivity assays showed that the SMC5/6 complex works in parallel
54 to the endonucleolytic and proteolytic pathways. The repair of zebularine-induced DPCs was
55 associated with SMC5/6-dependent SUMOylation of the damage sites. Thus, we present the
56 SMC5/6 complex as an important factor in plant DPC repair.

57

58 **IN A NUTSHELL**

59 **Background:** Cellular DNA is constantly damaged by various internal and external factors
60 that eventually lead to mutations, reduced growth or even death. To ensure genome stability,
61 organisms have evolved sophisticated and intricate DNA repair systems. We understand
62 how cells remove some types of DNA damage, but the mechanisms of detoxification from
63 other types of damage remain poorly characterized. For example, DNA-protein crosslinks,
64 i.e. proteins covalently attached to DNA molecule, hinder the essential processes of
65 replication and transcription.

66 **Question:** Our aim is to identify molecular factors protecting plants from toxic DNA-protein
67 crosslinks. We set up a forward-directed genetic screen to identify mutants hypersensitive to
68 the cytidine analog zebularine, which crosslinks DNA METHYLTRANSFERASE1 (MET1)
69 protein to the 45S rDNA repeats, and characterized the first candidate.

70 **Findings:** We mapped *HYPERSENSITIVE TO ZEBULARINE 1* (*HZE1*) candidate as
71 *SMC6B*, a core component of the Structural maintenance of chromosomes 5/6 (SMC5/6)
72 complex. *HZE1* plays a key role in DNA protein crosslink repair as it is needed for the repair
73 of different classes of crosslinks. We also showed that the SMC5/6 complex acts in parallel
74 with the known proteolytic and nucleolytic DNA-protein crosslink repair pathways. To shed

75 light on the possible mechanism of SMC5/6 action, we focused on the Small ubiquitin
76 modifier (SUMO) ligation activity of this complex. We showed the SMC5/6 complex-
77 dependent accumulation of SUMO at the crosslinked foci induced by zebularine.

78 **Next steps:** We will focus further on the role of SUMO in plant DNA damage repair and will
79 characterize other HZE candidates coming from the forward-directed genetic screen. This
80 will help us understand the mechanisms of DNA-protein crosslink repair in plants.

81

82 INTRODUCTION

83 Cellular DNA is constantly exposed to various genotoxic factors that may alter its
84 structure and result in DNA lesions. A common type of DNA damage is DNA-protein
85 crosslinks (DPCs), which form when proteins covalently bind to DNA. DPCs are among the
86 most toxic yet least studied lesions that impede DNA-related processes. Indeed, if not
87 repaired, DPCs may lead to mutations, genomic instability, and eventually cell death (Barker
88 et al., 2005). Based on their nature and origin, DPCs can be classified into three main
89 categories: enzymatic, non-enzymatic, and DPC-like traps (Zhang et al., 2020). Enzymatic
90 DPCs occur with proteins that form short-term covalent reaction intermediates as part of their
91 enzymatic cycle (e.g. topoisomerases, DNA methyltransferases). Such DPCs are formed by
92 stabilizing the covalent bond with a specific poison. Non-enzymatic DPCs are caused by the
93 covalent crosslinking of proteins located in the vicinity of DNA. Last, DPC-like trapping
94 occurs when a protein becomes firmly bound to DNA and behaves as a DPC (Stingele et al.,
95 2016, 2017; Klages-Mundt and Li, 2017; Weickert and Stingele, 2022).

96 Both endogenous and exogenous DPC inducers have been described. Endogenous
97 crosslinkers occur naturally in cells as products of metabolism and include reactive
98 aldehydes such as acetaldehyde and formaldehyde (Nakamura and Nakamura, 2020).
99 Exogenous crosslinkers are induced environmentally, e.g., after exposure to ultraviolet (UV)
100 or ionizing radiation (Kojima and Machida, 2020). Therapeutic crosslinkers represent
101 particular types of exogenous crosslinkers that were identified as potent chemotherapeutic
102 agents. Well-known examples of enzymatic poisons that intercalate at the DNA-protein
103 interface and cause covalent trapping of the target protein to DNA are camptothecin (CPT),
104 etoposide and 5-azacytidine or zebularine, which crosslink TOPOISOMERASE 1 (TOP1;
105 type-3 DPC) (Pommier and Marchand, 2012), TOPOISOMERASE 2 (TOP2; type-4 DPC)
106 (Nitiss et al., 2009), or DNA METHYLTRANSFERASE 1 (DNMT1/MET1; type-1 DPC)
107 (Maslov et al., 2012; Prochazkova et al., 2022), respectively.

108 Owing to the structural and chemical diversity of the proteins that can be crosslinked
109 and the DNA contexts in which they occur, DPCs can be challenging lesions for repair.
110 Several DPC repair pathways have been reported (Pouliot et al., 1999; Regairaz et al., 2011;

111 Stinglee et al., 2014; Sun et al., 2020a, 2020b). First, proteolytic cleavage of the protein
112 component of DPCs includes the recently-identified metalloproteases Weak suppressor of
113 Smt3 (Wss1) in yeasts and SPARTAN (SPRTN) in animals (Stinglee et al., 2016; Vaz et al.,
114 2016). Wss1/SPRTN proteolytic activity has no defined protein specificity but depends on
115 DNA binding. Second, direct enzymatic hydrolysis of the 3' phosphate from DNA and the
116 active tyrosyl residue of class I Topoisomerases was described, catalyzed by Tyrosyl-DNA
117 phosphodiesterase 1 (TDP1) in yeast *Saccharomyces cerevisiae* (Pouliot et al., 1999). Wss1
118 and TDP1 define parallel genetic pathways for the repair of CPT-induced DPCs in yeast
119 (Stinglee and Jentsch, 2015). The Arabidopsis (*Arabidopsis thaliana*) genome contains two
120 *Wss1* homologs, *WSS1A* and *WSS1B* (Enderle et al., 2019). However, only *wss1a* mutant
121 plants were hypersensitive to the DPC-inducing agents camptothecin (CPT) and cisplatin,
122 and no additive phenotype was observed in the *wss1a wss1b* double mutant. Therefore,
123 *WSS1A* is currently thought to be the only protease involved in the DPC repair in
124 Arabidopsis. Moreover, *wss1a* plants showed severe growth defects and reduced fertility,
125 probably due to the accumulation of natural DPCs. In contrast to animals, TDP1 only plays a
126 minor role in the repair of TOP1 crosslinks in Arabidopsis and may function as a backup
127 pathway to MUS81 and *WSS1A*-mediated repair (Enderle et al., 2019). Additionally, TDP2
128 contributes to the repair of TOP2 crosslinks in Arabidopsis (Hacker et al., 2022). Last, DPCs
129 can be directly processed by DNA endonucleases. The heterodimeric MMS AND UV
130 SENSITIVE 81 (MUS81) and ESSENTIAL MEIOTIC ENDONUCLEASE 1A (EME1)
131 endonuclease complex acts preferentially on DNA substrates that mimic stalled replication
132 forks, nicked Holliday junctions (HJs), and D-loops (Chen et al., 2001; Doe et al., 2002). In
133 Arabidopsis, MUS81 processes HJs, aberrant replication intermediates, and acts in
134 homologous recombination (HR) (Hartung et al., 2006; Mannuss et al., 2010). Plants lacking
135 MUS81 activity are hypersensitive to CPT and cisplatin, indicating their possible function in
136 processing DPCs next to single-strand breaks or stalled replication forks (Enderle et al.,
137 2019).

138 The STRUCTURAL MAINTENANCE OF CHROMOSOMES 5/6 (SMC5/6) complex is
139 an evolutionary conserved DNA-stimulated ATP-dependent molecular machine involved in
140 organizing DNA and preserving genome stability. The core SMC5/6 complex is composed of
141 the ring structure of SMC5 and SMC6 heterodimers and several NON-SMC ELEMENT
142 (NSE) subunits (Diaz and Pecinka, 2018; Palecek, 2019). The SUMO-ligase subunit NSE2 is
143 positioned at the SMC5 arm, and SUMOylates HR factors to stimulate DNA damage repair
144 (Varejão et al., 2018; Whalen et al., 2020). SUMO modification of DPCs also facilitates their
145 repair (Schellenberg et al., 2017; Borgermann et al., 2019) but has not been connected to
146 the SMC5/6 complex so far.

147 The Arabidopsis genome encodes two SMC6 (SMC6A, SMC6B), one SMC5 and six
148 NSE subunits (NSE1–3, NSE4A and NSE4B, ARABIDOPSIS SNI1 ASSOCIATED PROTEIN
149 1 [ASAP1], and SUPPRESSOR OF NPR1-1, INDUCIBLE 1 [SNI1]). However, only SMC6B,
150 NSE2, and NSE4A have been firmly associated with DNA damage repair (Watanabe et al.,
151 2009; Liu et al., 2015; Díaz et al., 2019). Our understanding of biological events controlled by
152 the plant SMC5/6 complex and its individual subunits is rather limited. Mutants defective in
153 each subunit are hypersensitive to DNA-damaging treatments, show delayed repair of DNA
154 strand breaks, and accumulate toxic replication intermediates originating during somatic and
155 meiotic HR (Liu et al., 2015; Diaz et al., 2019; Nowicka et al., 2020; Yang et al., 2021), but
156 the exact repair mechanism is unknown.

157 Recently, we showed that zebularine caused enzymatic DPCs in Arabidopsis by
158 covalently trapping the DNMT1 ortholog MET1 to DNA (Prochazkova et al., 2022). The
159 presence of zebularine-induced DPC is signaled by both ATM and ATR kinases (Liu et al.,
160 2015) and triggered genome instability (Nowicka et al., 2020). Here, we introduce a forward
161 genetic screen aimed at the identification of genes involved in the repair of zebularine-
162 induced DNA damage and present the first mapped complementation group
163 *HYPERSENSITIVE TO ZEBULARINE 1* (*HZE1*, pronounced as "haze", to refer to the long
164 unclear DNA damaging effects of zebularine). We mapped the high-effect candidate gene
165 *HZE1* to the *SMC6B* locus. Using several DNA-protein crosslinking agents and constructing
166 higher-order mutants, we show that SMC5/6 repairs DPCs in parallel to known DPC repair
167 pathways. Furthermore, our data suggest that the SUMOylation of MET1-DPCs by the
168 SMC5/6 complex is involved in DPC repair.

169 RESULTS

170 A forward genetic screening identifies *HZE1* as *SMC6B*

171 For the genetic screen, we mutagenized seeds of the Arabidopsis W35 line (Willing et
172 al., 2016) (hereby referred to as wild type, WT) with ethyl methanesulfonate (EMS) and
173 screened M2 seedlings for a decrease in root length when grown on half-strength Murashige
174 and Skoog (MS) medium containing 7.5 μ M zebularine. We validated the candidate mutant
175 using M₃ seedling grown in the presence of 20 μ M zebularine; we considered the candidates
176 as positive when showing at least a 60% reduction in root length compared to their mock-
177 treated control (for details, see Materials and Methods and Supplemental Figure S1). For
178 reference, the reduction in root length of treated WT seedlings relative to untreated WT was
179 40%. The first candidate identified in the screen showed an over 90% reduction in root length
180 (9.4% \pm 2.7% of mock-treated seedlings), indicating a strong sensitivity to zebularine (Figure
181 1A-C, Supplemental Table S1). We named this candidate *hze1-1* for *hypersensitive to*

182 *zebularine 1*. We performed mapping-by-sequencing (MBS) to identify the causal gene using
183 a pool of ~100 F₂ zebularine-sensitive seedlings derived from a backcross to WT
184 (Supplemental Figure S2A). We located the *hze1-1* mutation to the telomere-proximal region
185 on the bottom arm of chromosome 5 (Supplemental Figure S2B). We analyzed this region for
186 moderate to high-effect mutations within protein-coding regions and identified a G-to-A
187 transition in *SMC6B* at 3,627 bp downstream from the ATG (Figure 1D, Supplemental Figure
188 S2C), resulting in a D513N substitution. Notably, the putative causal mutation in *hze1-1* was
189 located within the *SMC6B* hinge domain (Figure 1E, 1F) in the highly conserved α -helix of
190 subdomain I (Alt et al., 2017) that is responsible for proper folding (Figure 1F). Homology
191 modeling using the budding yeast *SMC6B* crystal structure (Hallett et al., 2022) as template
192 revealed that the D513N substitution likely causes a subtle change in charge of the *SMC6B*
193 hinge domain, which may affect proper folding of the hinge domain (Figure 1F). We validated
194 *SMC6B* as the causal gene by analyzing sensitivity to zebularine in F₁ seedlings from a cross
195 between *hze1-1* and *smc6b-1*, which confirmed that *HZE1* is allelic to *SMC6B* (Supplemental
196 Figure S3).

197 To assess whether other mutant alleles in our collection affect *SMC6B*, we analyzed
198 the phenotypes of the remaining selected *hze* mutants on zebularine and found four
199 additional zebularine hypersensitive but otherwise phenotypically WT-like candidates. We
200 performed complementation crosses between these candidates and *smc6b-1*, followed by
201 zebularine sensitivity assays, which suggested that they are all allelic (Supplemental Figure
202 S3). Consequently, these candidates were named *hze1-2* to *hze1-5* (Figure 1A-D,
203 Supplemental Figure S3, Supplemental Table S1). We sequenced their *SMC6B* cDNA by
204 Sanger sequencing and modeled the effect of the identified substitutions using the *in silico*
205 predicted *SMC6B* structure (Figure 1D, 1E). In *hze1-2*, we detected a G-to-A transition 7,233
206 bp downstream of the *SMC6B* ATG, which overlapped with a splicing donor/acceptor site.
207 The *hze1-2* mutation resulted in alternative splicing of exon 28 that generated a 10-bp
208 deletion, introducing a premature stop codon in the sequence encoding the Walker B motif of
209 the ATPase head domain of *SMC6B* (Figure 1D, 1E). In *hze1-3*, we initially did not find any
210 mutations, but we failed to amplify one genomic region using primer pairs validated on WT
211 genomic DNA. We hypothesized that this region might be rearranged and therefore used
212 inverse PCR for isolation. Indeed, the sequencing of inverse PCR products suggested a
213 reciprocal translocation between chromosomes 5 and 4 with a breakpoint 5,472 bp
214 downstream of the *SMC6B* ATG and its fusion with a fragment of *NEXT TO BRCA1 GENE 1*
215 (*NBR1*) (Figure 1D, 1E, Supplemental Figure S4). We confirmed the translocation by a
216 standard PCR assay with individual primers positioned in *SMC6B* and *NBR1*, respectively
217 (Supplemental Figure S4). The *hze1-4* mutant carried a G-to-A transition 1,332 bp
218 downstream of the *SMC6B* ATG (Figure 1D, 1E, Supplemental Figure S3), which overlapped

219 with a splicing donor/acceptor site and resulted in the deletion of four amino acids (181–184,
 220 Δ FFFK) in the DNA-binding motif of the ATPase head domain SMC6B (Yu et al., 2022). The
 221 *hze1-5* mutant had a G-to-A transition 264 bp downstream of the *SMC6B* ATG (Figure 1D,
 222 1E, Supplemental Figure S3), which overlapped with a splicing donor/acceptor site and
 223 caused the retention of the 3rd intron in the final transcript. This retained intron added nine
 224 amino acids and a premature stop codon in the ATPase head domain (after amino acid 97).
 225 To exclude the possibility that sensitivity to zebularine was due to an SMC6B function
 226 independent from the SMC5/6 complex, we also tested *nse4a-2*, which carries a mutation in
 227 the kleisin subunit of the complex (Díaz et al., 2019) and confirmed its strong sensitivity to 20
 228 μ M zebularine (Figures 1A-C). Analyses of root cell viability using propidium iodide (PI)
 229 staining revealed an increased number of dead cells in the root meristematic zone of *hze1*
 230 and control *smc6b-1* and *nse4a-2* seedlings (Figure 1C). The *nse4a-2* seedlings showed
 231 fewer dead cells, most likely because this is not a null mutant allele (Díaz et al., 2019).

232 In conclusion, we identified five new EMS-induced *SMC6B* mutant alleles, *hze1-1* to
 233 *hze1-5* (corresponding to *smc6b-5* to *smc6b-9* alleles), and showed that the SMC5/6
 234 complex participates in the repair of zebularine-induced type-1 DPCs.

235 **The SMC5/6 complex is also involved in the repair of TOP1 and TOP2 DPCs**

236 The severity of *hze1* hypersensitivity to zebularine raised the question as to whether
 237 the SMC5/6 complex might also be involved in the repair of other types of DPCs.
 238 Accordingly, we analyzed root length in response to 20 nM CPT treatment. CPT crosslinks
 239 TOP1 and induces type-3 DPCs (Hacker et al., 2020). Root length in CPT-treated WT
 240 seedlings was 41.9% \pm 0.7% that of untreated control seedlings, while *smc6b-1* mutant
 241 seedlings displayed a significantly stronger reduction in root length, reaching only 23.4% \pm
 242 2.6 of the original root length (one-way ANOVA and Tukey's HSD post hoc test, $P < 0.05$;
 243 Figure 2A, C; Supplemental Table S2). In addition, CPT treatment shortened the
 244 meristematic zone and increased cell death in the roots of *smc6b-1* seedlings (Figure 2D).
 245 We observed a similar sensitivity in all tested *hze1* alleles (Figure 2A, 2B, 2D). Although
 246 *nse4a-2* seedlings showed a relatively strong reduction in root length (50.3% \pm 8.3%), this
 247 effect was not significantly different from that of WT seedlings ($P = 0.169$), consistent with the
 248 classification of the *nse4a-2* mutant as a hypomorphic allele (Díaz et al., 2019). In agreement
 249 with published data, we observed sensitivity to CPT for *mus81-1* and *wss1a-1* seedlings, but
 250 not for *tdp1-3* or *tdp2-5* (Supplemental Figure S5B, S5D, S5E) (Enderle et al., 2019; Hacker
 251 et al., 2022).

252 Second, we analyzed the role of the SMC5/6 complex in the repair of type-4 DPCs,
 253 typically associated with the crosslinking of TOP2 to its cleavage sites. This type of DPC is
 254 also caused by the TOP2 poison etoposide, which inhibits the religation of cleaved DNA

255 segments, resulting in TOP2 binding to the cleaved DNA ends (reviewed in Nitiss et al.,
256 2009). Because etoposide shortens root length only at very high concentrations (Hacker et
257 al., 2022), we screened several other TOP2 poisons and inhibitors used in mammalian
258 research and observed a strong effect after treatment with bisdioxopiperazine dexrazoxane
259 (ICRF-187) (Figure 2B-D, Supplemental Table S2). Seedlings from *smc6b-1*, *nse4a-2*, and
260 all tested *hze1* alleles (-1 to -3) showed a massive root length reduction to less than 25% of
261 mock-treated controls, while the root length in WT seedlings was only weakly affected in
262 response to 10 μ M ICRF-187, with a root length of $81.0\% \pm 1.7\%$ relative to the mock
263 treatment. In all cases with significantly reduced root length, we also detected more dead
264 cells in the root meristems of *smc6b-1*, multiple alleles of *hze1* and *nse4a-2* seedlings
265 (Figure 2D). We also observed hypersensitivity to ICRF-187 in *wss1a-1*, which was in
266 agreement with the known function of WSS1A in the repair of TOP2 crosslinks (Hacker et al.,
267 2022) (Supplemental Figure S5C-E, Supplemental Table S3). ICRF-187 is a highly-specific
268 TOP2 inhibitor that links the interface between two ATPase protomers of TOP2 (Classen et
269 al., 2003; Nitiss et al., 2009; Lee et al., 2017, 2022). To test the role of the SMC5/6 complex
270 in the repair of type-2 crosslinks, we tested several chemicals known to induce Poly (ADP-
271 ribose) polymerase 1 (PARP1) DPCs in mammalian cells (Waldman and Waldman, 1990;
272 Bernges and Zeller, 1996; Menear et al., 2008). However, there were no visible differences
273 between WT and *smc6b-1* (Supplemental Figure S6), preventing us from evaluating the
274 repair of type-2 crosslinks. Collectively, these findings provide strong evidence that the
275 SMC5/6 complex is a critical component in the repair of different types of DPCs and establish
276 ICRF-187 as a new drug for plant DPC repair research.

277 **SMC6B, MUS81, and WSS1A function non-redundantly during the repair of** 278 **endogenous DNA damage**

279 The endonuclease MUS81 and the protease WSS1A are required for DPC repair in
280 Arabidopsis (Enderle et al., 2019). To uncover a possible genetic interaction between the
281 SMC5/6 complex and these factors, we generated *mus81-1 smc6b-1* and *wss1a-1 smc6b-1*
282 double mutant plants and analyzed them under mock conditions with spontaneously
283 occurring DNA damage (Figure 3A, B, Supplemental Table S4). The root length of *smc6b-1*
284 ($1.18 \text{ cm} \pm 0.11$) and *mus81-1* ($1.41 \text{ cm} \pm 0.11$) seedlings was comparable to that of WT
285 seedlings ($1.34 \text{ cm} \pm 0.03$), while the roots of *wss1a-1* ($0.44 \text{ cm} \pm 0.05 \text{ cm}$) were significantly
286 shorter (one-way ANOVA and Tukey's HSD post hoc test, $P < 0.05$, note: the same test was
287 used throughout this section). The *smc6b-1 mus81-1* double mutant grown under mock
288 conditions showed a significant 75% reduction in root length ($0.31 \text{ cm} \pm 0.06 \text{ cm}$) relative to
289 mock-treated WT (Figure 3A, B). Furthermore, we observed more dead cells in the root
290 meristems of *smc6b-1 mus81-1* seedlings compared to WT and the respective single

291 mutants (Figure 3C). This increased number of dead cells was accompanied with modest
292 changes in root morphology (Figure 3C). The roots of *smc6b-1 wss1a-1* seedlings (0.14 cm \pm
293 0.01 cm) showed a drastic 90% length reduction relative to WT (Figure 3A, B), and their
294 anatomy was compromised with irregularly positioned and sized cells, a minimal
295 meristematic zone, and root hairs close to the root tip (Figure 3C). Although the total number
296 of dead cells in this double mutant appeared similar to that of *wss1a-1* seedlings (Figure 3C),
297 we speculate that this may reflect a bias caused by generally fewer cells in the root meristem
298 and transition zones. Adult *smc6b-1* and *mus81-1* single mutant plants were
299 indistinguishable from WT, but the *smc6b-1 mus81-1* double mutant showed severe growth
300 defects, including tiny rosettes and a shorter stem height by about 40% (Figure 3D, 3F).
301 Similarly, *smc6b-1 wss1a-1* double mutant plants also had a smaller rosette size and were
302 generally shorter compared to WT and single mutant controls (Figure 3D, 3F). Altogether,
303 these results indicate that the SMC5/6 complex functions in pathways parallel to MUS81
304 and/or WSS1A in the repair of spontaneously occurring DNA damage.

305 To explore whether the SMC5/6 complex contributes to both the MUS81 and WSS1A
306 pathways or whether it represents an independent yet unidentified pathway, we generated
307 the *smc6b-1 mus81-1 wss1a-1* triple mutant by crossing the above described homozygous
308 double mutant plants. We grew three independent *smc6b-1 mus81-1/MUS81 wss1a-1*
309 *1/WSS1a* F1 plants and expected 25% triple homozygous offspring upon selfing. However,
310 we obtained only 1% to 4% seedlings with the triple mutant genotype (2 out of 200, 4 out of
311 200, and 8 out of 200, in three independent replicates), indicating an additive effect on plant
312 lethality. Several triple homozygous mutant plants were at least partially fertile, allowing us to
313 analyze the phenotype of the progeny closer (Figure 3D, 3F). We selected the ten best-
314 looking plants for each double and triple mutant combinations from equally sized populations
315 (Figure 3D). The *smc6b-1 mus81-1 wss1a-1* plants showed stunted growth compared to the
316 respective double mutant plants, never developed proper roots or shoots, and were smaller
317 compared to the double mutants. Moreover, they were often dark-colored after prolonged
318 cultivation on MS medium (Figure 3F).

319 Based on these findings, we conclude that the SMC5/6 complex, MUS81, and
320 WSS1A function in at least partially unique pathways during the repair of spontaneously
321 occurring DNA damage.

322 **SMC5/6, MUS81, and WSS1A act additively during the repair of zebularine-induced** 323 **DPCs**

324 To uncover whether the SMC5/6 works together with MUS81 and WSS1A in the
325 repair of type-1 DPCs, we tested the zebularine sensitivity of *mus81-1 smc6b-1* and *wss1a-1*
326 *smc6b-1* double mutant plants, which revealed a dose-dependent phenotype (Figure 4A,

327 Supplemental Table S5). The double mutants showed a significant additive hypersensitivity,
328 compared to both single mutants, in response to a low zebularine concentration of 5 μ M
329 (one-way ANOVA and Tukey's HSD post hoc test, $P < 0.05$). On the contrary, a higher
330 zebularine concentration of 20 μ M fully inhibited *smc6b-1* growth, and we observed no
331 further enhancement of sensitivity in the double mutants. The PI staining of 20 μ M
332 zebularine-treated *smc6b-1 mus81-1* seedlings showed moderately altered root anatomy
333 with uneven cell files and a similar number of dead cells as in the root meristematic zone of
334 *smc6b-1* seedlings (Figure 4B). That differences are best observed at the lower zebularine
335 concentration for the fresh weight assay, and at the higher concentration in the cell death
336 assays reflects the different durations of these experiments.

337 WSS1/SPRTN proteins have a unique role in DPC repair (Stingele et al., 2016;
338 Reinking et al., 2020). Therefore, testing the sensitivity of *smc6b-1 wss1a-1* to zebularine
339 allowed us to unambiguously test the role of the SMC5/6 complex in DPC repair (Figure 4A,
340 Supplemental Table S5). Again, a high-dose zebularine treatment caused the greatest
341 sensitivity in *smc6b-1*, and we did not observe a further increase in the sensitivity of the
342 double mutants. For the 5- μ M zebularine dose, we measured a statistically significant
343 additive effect (one-way ANOVA and Tukey's HSD post hoc test, $P < 0.05$) in the *smc6b-1*
344 *wss1a-1* seedlings compared to the WT and respective single mutants. Due to the severely
345 affected root anatomy and a high number of dead cells under mock conditions, we could not
346 precisely estimate the effect of zebularine on the number of dead cells within the root
347 meristematic zone of *smc6b-1 wss1a-1* seedlings (Figure 4B). In general, the roots were
348 short and appeared very thick with minute meristematic zones. Because of the severe
349 developmental phenotype of the *smc6b-1 mus81-1 wss1a-1* triple mutants, we were not able
350 to analyze their response to zebularine.

351 In conclusion, our findings indicate that the SMC5/6 complex acts in a parallel
352 pathway to MUS81 for the repair of zebularine-induced DPCs. Moreover, we provide solid
353 genetic evidence that the SMC5/6 complex is specifically involved in DPC repair and
354 functions in the pathway(s) parallel to WSS1A protease.

355 **SUMOylation targets MET1 crosslinks in an SMC5/6-dependent manner**

356 In animals, proteins covalently trapped to DNA are targeted by SUMOylation
357 (Borgermann et al., 2019; Liu et al., 2021; Ruggiano et al., 2021). The SMC5/6 complex
358 contains the evolutionary conserved E3 SUMO ligase subunit NSE2 (Varejão et al., 2018).
359 Therefore, we wondered whether SMC6B might link the repair of zebularine-induced DPCs
360 with the SUMOylation activity of the SMC5/6 complex. We previously showed that zebularine
361 induces cytologically detectable DPC arrays at 45S rDNA in Arabidopsis by crosslinking a
362 large number of fluorescently-tagged MET1 (Prochazkova et al., 2022). To establish whether

363 zebularine-induced MET1-DPCs are targeted for SUMOylation, we analyzed SUMO
364 enrichment at MET1-RFP (red fluorescent protein) foci after zebularine treatment (Figure
365 5A). To this end, we performed immunolabeling with antibodies specific to SUMO1 or
366 SUMO3 on MET1-RFP positive nuclei isolated by flow sorting from mock- and zebularine-
367 treated wild-type plants as described (Prochazkova et al., 2022). We observed no
368 immunostaining of foci with antibodies against SUMO3 (Supplemental Figure S7). By
369 contrast, SUMO1 showed dispersed signals under mock conditions but largely colocalized
370 with MET1-RFP foci after a 40- μ M zebularine treatment (Figure 5A, 5B). To test whether
371 SMC5/6 is responsible for the zebularine-induced deposition of SUMO1 on MET1-DPCs, we
372 repeated the immunolabeling with the anti-SUMO1 antibody on MET1-RFP positive nuclei
373 from *smc6b-1* seedlings. Indeed, most zebularine-stimulated SUMO1 localization of MET1-
374 RFP foci was effectively abolished in the *smc6b-1* background (Figure 5A, B, D). Wild-type
375 plants showed 81% \pm 9% colocalization between MET1-RFP and SUMO1 signals upon
376 zebularine treatment, while *smc6b-1* reached only 22% \pm 4% (Figure 5D). To unequivocally
377 support a role for the SMC5/6 complex in SUMOylation at MET1-RFP foci, we repeated the
378 experiment with the *nse2-2 MET1-RFP* line. As with *smc6b-1*, about 24% \pm 3% of *nse2-2*
379 nuclei showed SUMO1 colocalization with MET1-RFP (Figure 5A, B, D).

380 This finding shows that the SMC5/6 complex adds SUMO1 to crosslinked MET1-RFP
381 upon zebularine treatment, thus highlighting the importance of the SMC5/6 complex in
382 SUMOylation of DPCs. The persistence of SUMO1 at around 20% of MET1-RFP foci also
383 suggests a role for another E3 SUMO ligase in labeling a subset of DPCs.

384 DISCUSSION

385 Here, we describe the SMC5/6 complex as an important component involved in the
386 repair of DNA-protein crosslinks, possibly through its E3 SUMO ligase activity. DPCs are
387 highly toxic DNA adducts that represent a major threat to the maintenance of genome
388 integrity (reviewed in Weickert and Stingle, 2022). DPCs, such as TOP1 crosslinks, are
389 formed during normal plant metabolism but are rapidly removed through a number of repair
390 pathways involved in their elimination. Unlike the repair of other types of DNA damage,
391 detoxification of DPCs has been studied in depth only recently (Stingle and Jentsch, 2015;
392 Vaz et al., 2016; Enderle et al., 2019; Larsen et al., 2019; Reinking et al., 2020; Liu et al.,
393 2021). In plants, three major DPC repair pathways have been described to date: the
394 nucleolytic pathway, which is hallmarked by the structure-specific endonuclease MUS81
395 (Enderle et al., 2019); the DPC-specific proteolytic pathway that depends on the
396 WSS1/Spartan metalloproteases (Stingle et al., 2016; Enderle et al., 2019); and the direct
397 hydrolytic pathway represented by TDP1 and TDP2 (Enderle et al., 2019; Tsuda et al.,

398 2020). We show that the SMC5/6 complex represents an independent or overarching DPC
399 repair pathway.

400 The function of the SMC5/6 complex is traditionally associated with DNA damage
401 repair and maintenance of genome stability. Using a forward genetic screen, we identified
402 five loss-of-function mutant alleles in *HYPERSENSITIVE TO ZEBULARINE 1 (HZE1)*, a
403 putative key player involved in the repair of zebularine-induced DPCs based on the strong
404 sensitivity of its mutants. The *HZE1* complementation group was allelic to *SMC6B*, a gene
405 encoding the core subunit of the SMC5/6 complex. The *hze1-2* mutant harbors a mutation in
406 the ATPase domain and most likely leads to a catalytically dead SMC6B. The *hze1-3* allele
407 carries a large translocation in the 3' end of the gene, effectively breaking the gene into two
408 fragments. The *hze1-4* allele lacks four amino acids in the ATPase head domain necessary
409 for interaction with DNA (Yu et al., 2022). Finally, the *hze1-1* allele represents a unique
410 mutation within subdomain I of the hinge region (Alt et al., 2017). Alignment of this region
411 from SMC6 homologs from different organisms revealed that it is highly conserved among
412 plant, fungal and animal species (Supplemental Figure S8). It is likely that the Asp-to-Asn
413 mutation in *hze1-1* results in aberrant chemical properties of the hinge domain, thus affecting
414 its structure and/or flexibility.

415 We selected the HZE mutants based on their sensitivity to zebularine, which is a
416 cytidine analog incorporated into DNA during replication and enables irreversible trapping of
417 the DNA methyltransferase MET1 in plants (Prochazkova et al., 2022). The exact repair
418 pathway of zebularine-MET1 DPCs is not known but sensitivity studies indicate that the
419 homologous recombination pathway is involved (Liu et al., 2015; Nowicka et al., 2020). The
420 isolation of *SMC6B* in our mutant screen is also in agreement with the role of the SMC5/6
421 complex, as SMC6B is required for efficient DNA damage repair by homologous
422 recombination (Mengiste et al., 1999; Potts et al., 2006; Watanabe et al., 2009). The
423 sensitivity to zebularine of a partial loss-of-function mutant in the kleisin subunit NSE4A
424 indicates that the SMC5/6 complex is involved in the DPC repair as a whole (Díaz et al.,
425 2019).

426 Here we show that the SMC5/6 complex is a universal player in DPC repair, as it was
427 not only involved in the repair of MET1 crosslinked to DNA by zebularine (representing type-
428 1 DPCs) but also in the repair of crosslinked TOP1 (type-3) and TOP2 (type-4).
429 Topoisomerases are enzymes that introduce transient DNA breaks to relax supercoiled or
430 intertwined DNA, thus allowing replication- and transcription-associated complexes to
431 proceed and sister chromatids to separate. In search of effective TOP2 inhibitors in plants,
432 we tested several compounds used for animal research and identified ICRF-187 as a new
433 highly potent crosslinker. The most substantial effects were when the drug was applied at
434 early stages of seedling development, possibly concomitant with the large number of

435 replicating nuclei. ICRF-187 crosslinks TOP2 in the ATP-associated state around double-
436 stranded DNA (dsDNA), hence creating a crosslink on DNA that is not associated with DNA
437 strand break (Classen et al., 2003; Lee et al., 2022). By contrast, cytidine analogs have a
438 very distinctive mode of action. Drugs like 5-azacytidine are incorporated into DNA and act
439 as a pseudosubstrate for DNA methyltransferases (DNMTs), resulting in the covalent
440 trapping of the enzyme without the primary presence of single-stranded (SSBs) or double-
441 stranded breaks (DSBs). Repairing such crosslinks may lead to DSBs (Maslov et al., 2012).
442 We did not observe increased sensitivity of *tdp1-3* or *tdp2-5* seedlings to zebularine-induced
443 DPCs. This result is in agreement with the fact that zebularine induces type-1 DPCs (Hacker
444 et al., 2020) that lack the phosphodiester bond, a common substrate for TDP1 and TDP2.
445 Therefore, the role of the SMC5/6 complex appears more general than that of other DPC
446 repair factors and likely DPC type-independent.

447 It is tempting to speculate how the SMC5/6 complex is involved in DPC repair (Figure
448 6). It has been shown that each of the two SMC6 homologs in Arabidopsis is required for the
449 efficient repair of DNA breakage via intermolecular homologous recombination in somatic
450 cells (Watanabe et al., 2009). Alignment of sister chromatids is enhanced transiently after X-
451 ray irradiation (and mitomycin C treatment) in WT nuclei. In the SMC5/6 complex mutants,
452 the X-ray-mediated increase in sister chromatid alignment is much lower and delayed than in
453 WT. Therefore, we hypothesize that the function of the SMC5/6 complex might be required
454 for the use of the sister chromatid as a template for repair. This mode of action might not only
455 be restricted to the repair of replicative DSBs by HR but also by post-replicative DPC repair
456 (Liu et al., 2021) in which a template-switching mechanism using the sister chromatid might
457 be involved (Torres-Ramos et al., 2002; Chen et al., 2008).

458 Interestingly, protein degradation by the proteasome in the replication-independent
459 pathway depends on the prior SUMOylation of the respective proteins (Liu et al., 2021).
460 Conjugation of SUMO has previously been described for several naturally occurring and
461 chemically-induced DPCs, including TOP1, TOP2, and DNMT1 in animals and yeast
462 (Schellenberg et al., 2017; Borgermann et al., 2019; Liu et al., 2021; Serbyn et al., 2021).
463 The E3 SUMO ligase activity of the SMC5/6 complex might mark crosslinked proteins for
464 degradation (Figure 6) and/or for conjugation with other factors promoting the repair. Hence,
465 SUMOylation via the SMC5/6 complex might be a mechanism integrating and orchestrating
466 various DPC repair pathways in plants. Interestingly, the SUMOylation activity of the SMC5/6
467 complex is unique among all SMC complexes and canonical DNA damage repair factors.
468 Arabidopsis genome encodes eight SUMO proteins, and four of the encoding genes are
469 expressed (*SUMO1*, 2, 3, 5) (Hammoudi et al., 2016). We discovered here that SUMO1, but
470 not SUMO3, is involved in DPC modification and that this is largely SMC5/6 complex-
471 dependent.

472 In summary, we identified SMC6B from our forward genetic screen for factors
473 contributing to the repair of zebularine-induced DNA-protein crosslinks. SMC6B is a core
474 subunit of the SMC5/6 complex that functions in several DPC repair pathways. We propose
475 that SUMOylation mediated by this complex plays an important role in DPC repair. Further
476 screening and identification of their candidates is in progress and provides a high potential to
477 identify and characterize additional DPC repair factors in Arabidopsis.

478 MATERIALS AND METHODS

479 Plant materials

480 Arabidopsis (*Arabidopsis thaliana*) wild type and mutants in the Col-0 background (unless
481 stated otherwise) were used in this study: *smc6b-1* (SALK_123114C), *nse4a-2* (GK-
482 768H08), *nse2-2* (SAIL_77_G06), *mus81-1* (GABI_113F11, (Hartung et al., 2006)), *wss1a-1*
483 (CRISPR/Cas9 line, (Enderle et al., 2019)), *tdp1-3* (CRISPR/Cas9 line with a 1-bp insertion
484 in exon 1 of *TDP1*, (Enderle et al., 2019)), *tdp2-5* (CRISPR/Cas9 line with a 5-bp deletion in
485 exon 1 of *TDP2*, (Hacker et al., 2022)). The double mutants were generated by crossing
486 homozygous single mutants and identification in the F2 generation by PCR-based
487 genotyping. Plants homozygous for the *wss1a-1* mutation were identified by Sanger
488 sequencing of PCR products spanning the mutated site. The primers used for genotyping are
489 listed in Supplemental Table S7. Plants were cultivated in an air-conditioned phytochamber
490 under a long-day photoperiod (16-h light, 150 $\mu\text{mol m}^{-2} \text{s}^{-1}$, 21°C, 8-h dark, 19°C; lights
491 provided by fluorescent tubes MASTER TL-D 18W/840, Philips). For the drug sensitivity
492 assays, seeds were surface-sterilized using 8% (w/v) sodium hypochlorite solution for 6 min,
493 followed by three washes in sterile H₂O, stratification for 2 days at 4°C in the dark. Seeds
494 were evenly distributed on plates containing half-strength Murashige and Skoog medium
495 (MS) with 0.6% (w/v) agar and with or without the addition of DNA-protein crosslinking
496 chemicals, depending on the experimental setup.

497 DCPR forward-directed genetic screen setup, candidate mapping-by-sequencing 498 (MBS), and inverse PCR

499 For the HZE genetic screen (Supplemental Figure S1), an ethyl methanesulfonate (EMS)-
500 mutagenized population was used in the W35 reporter line (Col-0 carrying *ProUVR2:UVR2-
501 LUCIFERASE*) background (Willing et al., 2016). The reporter line behaves as wild type, and
502 *UVR2* expression was not monitored in this study. About 10,000 seeds were soaked in 0.1%
503 (w/v) KCl and shaken at 4°C for 8 h; seeds were then washed in distilled water and
504 incubated in 0.2% (v/v) EMS solution at room temperature for 12 h to induce mutations.
505 Afterwards, seeds were washed 2 × 5 min with 100 mM sodium thiosulfate and 3 × 5 min
506 with water. Finally, the seeds were resuspended in 0.1% (w/v) agarose and spread onto soil
507 surface at a density of ~100 seeds per 18 × 14 cm tray. All M1 plants were grown until

508 maturity; seeds of all plants from one tray were collected together, resulting in 100 M2 seed
509 batches. Approximately 1,500 seeds per M2 batch were surface-sterilized with 8% (w/v)
510 sodium hypochlorite for six min, followed by three washes with sterile water, resuspension in
511 0.1% (w/v) agarose, and 1,600 seeds were evenly sown onto plates filled with half-strength
512 MS medium containing 20 μ M zebularine using a pipette with a sterile cut plastic tip. Each
513 plate included the zebularine-sensitive control *smc6b-1* and resistant wild-type controls.
514 Seedlings were grown in a phytochamber under long-day conditions for 10 days. Afterwards,
515 the plates were visually inspected, and primary candidates with short roots were transferred
516 to soil and grown until maturity, and their M3 seeds were collected. Each primary M2
517 candidate was further analyzed by phenotyping the M3 generation on half-strength MS
518 medium without or with 20 μ M zebularine (approximately 30 seedlings per experimental
519 point). Based on the phenotype, each candidate was classified into one of the following
520 categories: (i) developmental mutants with short roots on both control and zebularine-
521 containing media; (ii) false positive with less than a 60% reduction in root length on control
522 medium compared to zebularine-containing medium; (iii) true candidates with at least a 60%
523 reduction in root length on control medium compared to zebularine-containing medium. Only
524 type (iii) candidates were considered for further work.

525 The candidates selected for mapping were backcrossed to the non-mutagenized wild
526 type Col-0, and the resulting F2 population was screened on half-strength MS medium
527 containing 20 μ M zebularine. Segregation of the zebularine-sensitive phenotype was
528 assessed, which typically matched the expected segregation pattern for a single nuclear
529 recessive locus. About 75 to 150 zebularine-sensitive seedlings were collected, pooled, and
530 their genomic DNA was isolated using a NucleoSpin Plant II kit (Macherey-Nagel). Genomic
531 DNA was sent for sequencing (Novogene LTD, Cambridge, UK), as paired-end 150-bp reads
532 on a Novaseq platform to approximately 50x coverage. Sequencing data were analyzed
533 using bioinformatics tools available at the public platform usegalaxy.org as described
534 (Prochazkova et al., 2022). The clean reads were mapped to the *Arabidopsis thaliana*
535 reference genome (TAIR10) with bowtie2 using default settings (Langmead et al., 2009;
536 Langmead and Salzberg, 2012). Read sorting, SNP calling, and filtering were performed
537 using tools from the MiModD tool set (<https://celegans.de/mimodd/>) and annotated with the
538 snpEff tool (Cingolani et al., 2012). Sequencing data of the mapping populations were
539 deposited at the NCBI Sequence Read Archive under accession number PRJNA730368.
540 Mapping information of respective candidates was uploaded to the UCSC Genome Browser
541 with the following IDs: [http://genome-](http://genome-euro.ucsc.edu/s/KlaProche/candidate%208%2D13%20a.k.a.%20dpcr1)
542 [euro.ucsc.edu/s/KlaProche/candidate%208%2D13%20a.k.a.%20dpcr1](http://genome-euro.ucsc.edu/s/KlaProche/candidate%208%2D13%20a.k.a.%20dpcr1).

543 The *SMC6B* locus was sequenced in the candidates identified as *smc6b* mutants via
544 complementation crosses with *smc6b-1*. Total RNA extraction and first-strand cDNA

545 synthesis were performed as described previously (Nowicka et al., 2020). The *SMC6B*
546 transcript was divided into six regions, amplified with specific primers (Supplemental Table
547 S1) and PCR products were sequenced by Sanger sequencing. To identify the putative
548 rearranged region in *hze1-3*, inverse PCR was performed. Briefly, 2 µg genomic DNA was
549 digested with 10 units of *Xmnl* for 1 h, 50 ng of linear DNA was religated with 5 units of T4
550 DNA ligase for 1 h at room temperature, and the sample was used as a template for
551 amplification with *SMC6B*-specific primers. The resulting PCR product was cleaned with
552 ExoSAP-IT™ PCR Product Cleanup Reagent (Thermo Fisher) and sequenced by Sanger
553 sequencing.

554 **Root length assays and phenotypical analyses of mutant plants**

555 Stratified, surface-sterilized seeds were evenly sown on square culture plates with half-
556 strength MS medium with 0.8% (w/v) agar, and placed horizontally for 7 d. Subsequently, the
557 seedlings were carefully pulled off the agar surface with tweezers and stretched onto fresh
558 agar plates. Seedlings were photographed with a D90 digital camera (Nikon), and the length
559 of the primary root was measured using the ImageJ plugin SmartRoot (Lobet et al., 2011).
560 Detailed photographs were collected using an SZX16 binocular microscope equipped with a
561 Regita 1300 QImaging camera and QCapture x64 software (both Olympus).

562 For sensitivity assays of single mutants, seeds were germinated on half-strength MS medium
563 with 0.8% (w/v) agar containing individual chemicals: 20 µM zebularine (Z4775, Sigma-
564 Aldrich), 20 nM (S)-(+)-camptothecin (CPT, C9911, Sigma-Aldrich), 10 µM ICRF-187 (D1446,
565 Sigma-Aldrich), 100 nM, 10 µM and 100 µM AZD2461 (SML1858, Sigma-Aldrich), 100 nM,
566 100 µM and 1 mM 3-methoxybenzamide (M10050, Sigma-Aldrich), 100 µM, 1 mM and 4 mM
567 3-aminobenzamide (A0788, Sigma-Aldrich). Sensitivity to each chemical treatment in
568 individual replicates was determined by calculating mean (treatment) / mean (mock). The
569 experiment was performed as three biological replicates, each with at least 20
570 seedlings/replicate. The means of the three replicates are shown. Statistical significance was
571 tested by one-way analysis ANOVA with post-hoc Tukey HSD in R (Core R Team, 2020).

572 **Drug sensitivity assays**

573 Drug sensitivity assays were performed as described (Dorn and Puchta, 2020). Stratified,
574 surface-sterilized seeds were sown on culture plates with half-strength MS medium with
575 0.6% (w/v) agar, and cultivated for seven days. Subsequently, ten seedlings of each
576 genotype were transferred to a six-well culture plate containing 5 mL of liquid half-strength
577 MS medium (untreated control) or 4 mL of liquid half-strength MS medium (treated samples)
578 per well under sterile conditions. The next day, 1 ml of genotoxin solution diluted in liquid
579 half-strength MS medium was added to obtain the desired final concentration. Seedling fresh
580 weight was measured after 13 days of exposure. Relative fresh weight was determined by

581 comparison of fresh weight between treated and untreated samples for each genotype and
582 concentration. The experiment was performed as three biological replicates, and the means
583 of the three replicates are shown.

584 **Cell death analyses in roots**

585 Seeds were sown on plates containing half-strength MS medium with 0.6% (w/v) agar and
586 grown vertically for five days before transfer to liquid half-strength MS medium without
587 (mock) or with 20 μ M zebularine, 20 nM CPT or 10 μ M ICRF-187 for 24 h. Afterwards, the
588 seedlings were placed in 10 mg mL⁻¹ propidium iodide (PI, Sigma) on slides and immediately
589 analyzed and photographed using a Leica confocal microscope TCS SP8 (Leica, Wetzlar,
590 Germany) and HC PL APO CS2 20x/0.75 DRY objective equipped by Leica LAS-X software
591 with Leica Lightning module laser scanning confocal microscope (Leica). The pattern was
592 checked in at least ten individual seedlings per treatment.

593 **Immunostaining and confocal microscopy**

594 Immunostaining was performed as previously described (Prochazkova et al., 2022). Briefly,
595 5-day-old seedlings were incubated in 0 (mock) or 40 μ M zebularine for 24 h. Seedlings were
596 fixed with 4% (w/v) formaldehyde in Tris buffer (10 mM Tris-HCl pH 7.5, 10 mM NaEDTA,
597 100 mM NaCl) at 4°C for 20 min and washed 2 \times 10 min with Tris buffer at 4°C. Seedlings
598 were chopped in 500 μ L LB01 buffer and filtered through 50- μ m and 20- μ m cell strainer
599 caps. Flow cytometry analysis and sorting were carried out on a FACSAria II SORP flow
600 cytometer and sorter (Becton Dickinson Immunocytometry Systems, San José, USA). The
601 samples were analyzed at rates of 400–1,400 particles per second. Bivariate flow karyotypes
602 of PI pulse area (PI-A) vs. DAPI pulse area (DAPI-A) fluorescence were acquired, and
603 20,000 events were recorded to create a bivariate flow karyotype for each experiment.
604 Sorted regions were set on the flow karyotypes, and RFP-positive nuclei were sorted onto
605 microscope slides with a 3- μ L drop of PRINS buffer supplemented with 2.5% (w/v) sucrose
606 (Kubaláková et al., 1997). Around 3,000 nuclei were sorted per slide. Slides were post-fixed
607 with 4% (w/v) formaldehyde in phosphate-buffered saline (PBS) for 15 min and washed with
608 PBS. For immunolocalization of SUMO1 and SUMO2/3, slides were incubated with a rabbit
609 anti-SUMO1 or anti-SUMO3 primary antibody diluted 1:200 (ab5316 and ab5317, Abcam) at
610 4°C overnight, and a goat anti-rabbit Alexa Fluor 488-conjugated secondary antibody diluted
611 1:250 (A11008, Invitrogen) at room temperature for 2 h. The slides were shortly washed with
612 1 \times PBS, and nuclei were counterstained with DAPI (300 ng. μ L⁻¹) and mounted in
613 Vectashield (H-1000, Vector Laboratories). Imaging was performed with a Leica confocal
614 microscope TCS SP8 (Leica 265 Microsystems) and HC PL PAO CS2 63 \times /1.4 OIL objective
615 equipped with Leica LAS-X software (Leica). Images were captured separately for each
616 fluorochrome with 546-nm (MET1-RFP), 488-nm (Alexa Fluor 488), and 405-nm (DAPI) laser

617 lines for excitation and appropriate emission filters. Processing of the final images and
618 quantitative analysis of MET1-RFP colocalization with SUMO1 was performed in ImageJ
619 using a fluorescent intensity profile for both correlated signals. The respective colocalization
620 coefficients were calculated by Pearson's correlation coefficient in Microsoft Excel.

621 **Multiple sequence alignment**

622 Multiple sequence alignment was performed to elucidate the conservation level of mutations
623 in SMC6B. Sequence data of the proteins used in Supplemental Figure S8 were retrieved
624 from UniProt: Q9FII7 (*Arabidopsis* SMC6B), Q9FLR5 (*Arabidopsis* SMC6A), D7MV22
625 (*Arabidopsis lyrata* SMC6B), P53692 (*Schizosaccharomyces pombe* SMC6), Q12749
626 (*Saccharomyces cerevisiae* SMC6), Q96SB8 (*Homo sapiens* SMC6), Q8GU52 (*Oryza sativa*
627 SMC6), A0A0Q3L328 (*Brachypodium distachyon* SMC6), M4D8Z6 (*Brassica rapa* SMC),
628 R0G894 (*Capsella rubella* SMC), A0A1S3ZHR2 (*Nicotiana tabacum* SMC6), A0A3Q7GL50
629 (*Solanum lycopersicum* SMC6), A0A2K2B516 (*Populus trichocarpa* SMC6), D7U753 (*Vitis*
630 *vinifera* SMC6). Analyses were performed in the AliView program (Larsson, 2014).

631 **Protein structure analysis**

632 The model of AtSMC6B subunit (UniProt ACC: Q9FIIH) was built using SWISS-MODEL
633 (Bienert et al., 2017; Waterhouse et al., 2018). ScSMC6 (PDBID: 7qcd) (Hallett et al., 2022)
634 was used as a template. More detailed hinge models were generated using AlphaFold2. All
635 models were further processed in PyMOL (Schrödinger, LLC, 2015).

636 **Statistical methods**

637 To determine statistically significant effects, one-way analysis of variance (ANOVA) with
638 post-hoc Tukey HSD ($P \leq 0.05$) tests were performed in R (Core R Team, 2020). Statistical
639 significance of colocalization between MET1-RFP and SUMO1 in the wild-type, *smc6b-1*,
640 and *nse2-2* backgrounds was calculated with a chi-square test.

641 **Accession numbers**

642 Sequencing data of the mapping populations were deposited at the NCBI Sequence Read
643 Archive under accession number PRJNA730368. Sequence data of the genes used in this
644 article can be found at TAIR under the following accession numbers: *SMC6B* (At5g61460),
645 *NSE4A* (At1g51130), *NSE2* (At3g15150), *MUS81* (At4g30870), *TDP1* (At5g15170), *TDP2*
646 (At1g11800), *WSS1A* (At1g55915).

647 **Acknowledgments**

648 We thank Helena Tvardíková and Eva Jahnová for excellent technical assistance, Zdeňka
649 Bursová for plant care. The Czech Science Foundation supported EDT, KP, FY, and AP by
650 grant 22-00871S, JJ was supported by grant GA20-05095S. AP and FY also received
651 funding from the Czech Academy of Sciences (Purkyně fellowship and PPPLZ, respectively).

652 At the MIPZ Cologne, AP and AF were supported by core funding from the Max Planck
653 Society. Computational resources were provided by the project "e-Infrastruktura CZ" (e-
654 INFRA CZ LM2018140) supported by the Ministry of Education, Youth, and Sports of the
655 Czech Republic.

656 The authors declare no conflict of interest.

657 **Authors contributions**

658 AP, EDT, AF, and HP designed the research, EDT, FY, AF, KP, JJ, and MS performed the
659 analysis, AD, and HP developed CRISPR mutant, EDT, FY, KP, JJ, and AP analyzed the
660 data. EDT and AP wrote the article.

661

662

663

664

665

666

667

668

669

670

671

672

673

674

675

676

677

678

679

680

681

682

ACCEPTED MANUSCRIPT

683
684
685
686
687
688
689
690
691

692 Figure legends

693 **Figure 1.** *HYPERSENSITIVE TO ZEBULARINE 1 (HZE1)* encodes the SMC5/6 complex
694 subunit SMC6B.

695 A, Representative growth phenotypes of seedlings from wild type (WT), *smc6b-1*, *hze1*
696 alleles and *nse42-2* on 0 (Mock) and 20 μ M zebularine (ZEB). Scale bar, 1 cm. B, Relative
697 root length of seedlings in (A) under zebularine/mock conditions (% of ZEB/Mock). Data are
698 means \pm SD from three biological replicates, each with a minimum of 14 seedlings. Different
699 lowercase letters indicate significant differences ($P < 0.05$), according to one-way ANOVA
700 followed by Tukey's test. Source data for statistical analyses are available in Supplemental
701 Table S1. The original experiment was split between Figures 1A-C, and Supplemental
702 Figures S5A-D. Therefore, these figures show identical images and data for the controls. C,
703 Representative confocal microscopy images of root tips stained with propidium iodide, which
704 indicates dead cells (dark sectors). Five-day-old seedlings were treated with 20 μ M ZEB for
705 24 h prior to analysis. Scale bar, 100 μ m. D, Schematic model of the *SMC6B/HZE1* locus
706 (At5g61460) with the positions of individual mutations. E, Detailed position of *hze1-1* to *hze1-5*
707 mutations (magenta) in the AtSMC6B protein structure. The AtSMC6B (UniProt ACC:
708 Q9FIIH) model was built using SWISS-MODEL using *Saccharomyces cerevisiae* SMC6
709 (PBDID: 7qcd) (Hallett et al., 2022) as template. F, Superposed models of the hinge domain
710 from wild-type SMC6B (azure) and SMC6B in *hze1-1* (green) generated using AlphaFold2.
711 Position of the D513N substitution is marked with black circle. The predicted effect on
712 secondary structure is marked with black asterisks.

713

714 **Figure 2.** The SMC5/6 complex is required for the repair of type-3 and type-4 DNA protein
715 crosslinks (DPCs).

716 A, Representative growth phenotype of wild-type (WT) and mutant seedlings on medium
717 without DPC inducers (Mock) or containing 20 nM camptothecin (CPT) or 10 μ M ICRF-187
718 (ICRF). Scale bar, 1 cm. B, C, Relative root length of WT and mutant seedlings grown in the
719 presence of 20 nM CPT (B) or 10 μ M ICRF (C). Data are means \pm SD from three biological
720 replicates, each with at least 20 seedlings. Different letters indicate significant differences (P
721 < 0.05) according to one-way ANOVA followed by Tukey's test. Source data for statistical
722 analyses are available in Supplemental Table S2. The original experiment was split between
723 Figure 2A-C and Supplemental Figures S5A-D. Therefore, these figures show identical
724 images and data for the controls. D, Representative confocal microscopy images of root
725 apices stained with propidium iodide. Five-day-old seedlings were treated for 24 h with 20
726 nM PT or 10 μ M ICRF prior to analysis. Dark sectors within the roots indicate dead cells.
727 Scale bar, 100 μ m.

728
729
730
731
732
733
734
735
736
737
738
739
740
741
742
743
744

Figure 3. Phenotypic analysis of *smc6b-1*, *mus81-1*, *wss1a-1* and their higher-order mutants under normal conditions. A, Representative growth phenotype of wild type, *smc6b-1*, *mus81-1*, *wss1a-1* and double mutants with *smc6b-1*. Scale bar, 1 cm. B, Quantification of root length from A. At least 20 roots per genotype were analyzed in each of three biological replicates. The lower and upper hinges of the boxplots correspond to the first and third quartiles of the data, the black lines within the boxes indicates the median. Whiskers mark 10% and 90% intervals. Different letters indicate significant differences ($P < 0.05$) according to one-way ANOVA followed by Tukey's test. Source data for statistical analyses in B are available in Supplemental Table S4A. C, Representative confocal microscopy images of root tips stained with propidium iodide. Seedlings were grown for five days on control medium prior to analysis. Dark sectors indicate dead cells. Scale bar, 100 μm . D, Representative phenotypes of two-week-old WT, single mutants, double mutants, and *smc6b-1 mus81-1 wss1a-1* triple mutant seedlings grown on half-strength MS medium. Scale bar, 1 cm. E, Detailed photograph of three-week-old *smc6b-1 mus81-1 wss1a-1* triple mutant seedlings with severe phenotype grown on half-strength MS medium. Scale bar, 1 cm. F, Representative phenotypes of six-week old plants grown on soil. Scale bar, 70 mm.

745

746 **Figure 4.** Sensitivity of *smc6b-1 mus81-1* and *smc6b-1 wss1a-1* plants to zebularine.
747 A, Fresh weight of plants treated with 5 μM or 20 μM zebularine (ZEB). The sensitivity of
748 double mutant plants was compared to the respective single mutants and WT plants relative
749 to the mock-treated plants of the same genotype. Data are means \pm SD of three biological
750 replicates. Different letters indicate significant differences ($P < 0.05$) according to one-way
751 ANOVA followed by Tukey's test. Source data for A are available in Supplemental Table S4.
752 B, Representative confocal microscopy images of root tips stained with propidium iodide.
753 Scale bar, 100 μm .

754

755 **Figure 5.** SMC5/6-dependent SUMOylation of zebularine-induced MET1 crosslinks.
756 A, Immunolabeling of mock- and zebularine-treated WT, *smc6b-1*, and *nse2-2* root nuclei
757 stained with SUMO1 antibody. MET1-RFP signals were observed directly, and nuclei were
758 counterstained with DAPI. The white lines in Merge indicate intersects for fluorescence
759 intensity measurements shown in (B). Scale bar, 5 μm . B, Fluorescence intensity (FI) plots
760 based on the white lines indicated intersects in (A). The y-axis shows FI intensity in arbitrary
761 units (AU) for MET1-RFP and SUMO1 signals. R indicates Pearson's correlation coefficient
762 assessment of colocalization (1, full colocalization). C, Detailed image of MET1-RFP
763 colocalization with SUMO1 (from A) in WT nuclei after zebularine treatment. Scale bar, 1 μm .
764 D, Percentage of nuclei with MET1-RFP foci colocalizing with SUMO1 in WT, *smc6b-1* and
765 *nse2-2* root nuclei after zebularine treatment. Data are means \pm SD from three biological
766 replicates. Statistical significance was tested with chi-square test (*smc6b-1* χ^2 (2, N = 544) =
767 196.6331, $p = .000$, *nse2-2* (χ^2 (2, N = 651) = 231.7348, $p = .000$). n, total number of nuclei
768 evaluated per genotype. Source data for the analyses are available in Supplemental Table
769 S6.

770

771 **Figure 6.** Working model of zebularine-induced DPC repair. The endonuclease MUS81
772 cleaves DNA surrounding the crosslink. The SMC5/6 complex deposits SUMO residues on
773 the MET1-DPC or adjacent repair proteins to stimulate repair. Without the SMC5/6 complex,
774 the protease WSS1A proteolytically degrades the protein crosslinked by zebularine.

775
776
777
778
779
780
781
782
783
784
785
786
787
788
789
790
791
792
793
794
795
796
797
798
799
800
801
802
803
804
805
806
807
808
809
810
811

References

- Alt, A., Dang, H.Q., Wells, O.S., Polo, L.M., Smith, M.A., McGregor, G.A., Welte, T., Lehmann, A.R., Pearl, L.H., Murray, J.M., and Oliver, A.W.** (2017). Specialized interfaces of Smc5/6 control hinge stability and DNA association. *Nat Commun* **8**, 14011.
- Barker, S., Weinfeld, M., and Murray, D.** (2005). DNA–protein crosslinks: their induction, repair, and biological consequences. *Mutat Res* **589**: 111–135.
- Bernges, F. and Zeller, W.J.** (1996). Combination effects of poly(ADP-ribose) polymerase inhibitors and DNA-damaging agents in ovarian tumor cell lines—with special reference to cisplatin. *J Cancer Res Clin Oncol* **122**: 665–670.
- Bienert, S., Waterhouse, A., De Beer, T.A.P., Tauriello, G., Studer, G., Bordoli, L., and Schwede, T.** (2017). The SWISS-MODEL Repository—new features and functionality. *Nucleic Acids Res* **45**: D313–D319.
- Borgermann, N., Ackermann, L., Schwertman, P., Hendriks, I.A., Thijssen, K., Liu, J.C., Lans, H., Nielsen, M.L., and Mailand, N.** (2019). SUMOylation promotes protective responses to DNA -protein crosslinks . *EMBO J* **38**: e101496.
- Chen, X.B., Melchionna, R., Denis, C.M., Gaillard, P.H.L., Blasina, A., Van de Weyer, I., Boddy, M.N., Russell, P., Vialard, J., and McGowan, C.H.** (2001). Human Mus81-associated endonuclease cleaves Holliday junctions in vitro. *Mol Cell* **8**: 1117–1127.
- Chen, Z., Yang, H., and Pavletich, N.P.** (2008). Mechanism of homologous recombination from the RecA–ssDNA/dsDNA structures. *Nature* **453**: 489–494.
- Cingolani, P., Platts, A., Wang, L.L., Coon, M., Nguyen, T., Wang, L., Land, S.J., Lu, X., and Ruden, D.M.** (2012). A program for annotating and predicting the effects of single nucleotide polymorphisms, SnpEff: SNPs in the genome of *Drosophila melanogaster* strain w1118; iso-2; iso-3. *Fly (Austin)*. **6**: 80–92.
- Classen, S., Olland, S., and Berger, J.M.** (2003). Structure of the topoisomerase II ATPase region and its mechanism of inhibition by the chemotherapeutic agent ICRF-187. *Proc Natl Acad Sci U S A* **100**: 10629–10634.
- Core R Team** (2020). A language and environment for statistical computing. *R Found. Stat. Comput.* **2**: <https://www.R-project.org>.
- Díaz, M. et al.** (2019). The SMC5/6 complex subunit NSE4A is involved in DNA damage repair and seed development. *Plant Cell* **31**: 1579–1597.
- Diaz, M. and Pecinka, A.** (2018). Scaffolding for repair: understanding molecular functions of the SMC5/6 complex. *Genes (Basel)*. **9**: 36.
- Diaz, M., Pecinkova, P., Nowicka, A., Baroux, C., Sakamoto, T., Gandha, P.Y., Jeřábková, H., Matsunaga, S., Grossniklaus, U., and Pecinka, A.** (2019). SMC5/6

- 812 Complex Subunit NSE4A is Involved in DNA Damage Repair and Seed Development in
813 Arabidopsis. *Plant Cell* **31**: 1579-1597. **Doe, C.L., Ahn, J.S., Dixon, J., and Whitby,**
814 **M.C.** (2002). Mus81-Eme1 and Rqh1 involvement in processing stalled and collapsed
815 replication forks. *J Biol Chem* **277**: 32753–32759.
- 816 **Dorn, A. and Puchta, H.** (2020). Analyzing somatic DNA repair in Arabidopsis meiotic
817 mutants. *Methods Mol Biol* **2061**: 359-366.
- 818 **Enderle, J., Dorn, A., Beying, N., Trapp, O., and Puchta, H.** (2019). The protease WSS1A,
819 the endonuclease MUS81, and the phosphodiesterase TDP1 are involved in
820 independent pathways of DNA-protein crosslink repair in plants. *Plant Cell* **31**: 775–790.
- 821 **Hacker, L. et al.** (2020). Repair of DNA-protein crosslinks in plants. *DNA Repair (Amst)*. **87**:
822 102787.
- 823 **Hacker, L., Dorn, A., Enderle, J., and Puchta, H.** (2022). The repair of topoisomerase 2
824 cleavage complexes in Arabidopsis. *Plant Cell* **34**: 287–301.
- 825 **Hallett, S.T., Harry, I.C., Schellenberger, P., Zhou, L., Cronin, N.B., Baxter, J.,**
826 **Etheridge, T.J., Murray, J.M., and Oliver, A.W.** (2022). Cryo-EM structure of the Smc5
827 / 6 holo-complex. *Nucleic Acids Res* **50**: 9505–9520.
- 828 **Hammoudi, V., Vlachakis, G., Schranz, M.E., and van den Burg, H.A.** (2016). Whole-
829 genome duplications followed by tandem duplications drive diversification of the protein
830 modifier SUMO in Angiosperms. *New Phytol.* **211**: 172–185.
- 831 **Hartung, F., Suer, S., Bergmann, T., and Puchta, H.** (2006). The role of AtMUS81 in DNA
832 repair and its genetic interaction with the helicase AtRecQ4A. *Nucleic Acids Res.* **34**:
833 4438–4448.
- 834 **Klages-Mundt, N.L. and Li, L.** (2017). Formation and repair of DNA-protein crosslink
835 damage. *Sci China Life Sci* **60**: 1065–1076.
- 836 **Kojima, Y. and Machida, Y.J.** (2020). DNA-protein crosslinks from environmental exposure:
837 Mechanisms of formation and repair. *Environ Mol Mutagen* **61**: 716–729.
- 838 **Kubaláková, M., Macas, J., and Doležel, J.** (1997). Mapping of repeated DNA sequences
839 in plant chromosomes by PRINS and C-PRINS. *Theor Appl Genet* **94**: 758–763.
- 840 **Langmead, B. and Salzberg, S.L.** (2012). Fast gapped-read alignment with Bowtie 2. *Nat*
841 *Methods* **9**: 357–359.
- 842 **Langmead, B., Trapnell, C., Pop, M., and Salzberg, S.L.** (2009). Ultrafast and memory-
843 efficient alignment of short DNA sequences to the human genome. *Genome Biol* **10**:
844 R25.
- 845 **Larsen, N.B., Gao, A.O., Sparks, J.L., Gallina, I., Wu, R.A., Mann, M., Räschle, M.,**
846 **Walter, J.C., and Duxin, J.P.** (2019). Replication-Coupled DNA-Protein Crosslink
847 Repair by SPRTN and the Proteasome in *Xenopus* Egg Extracts. *Mol Cell* **73**: 574-
848 588.e7.

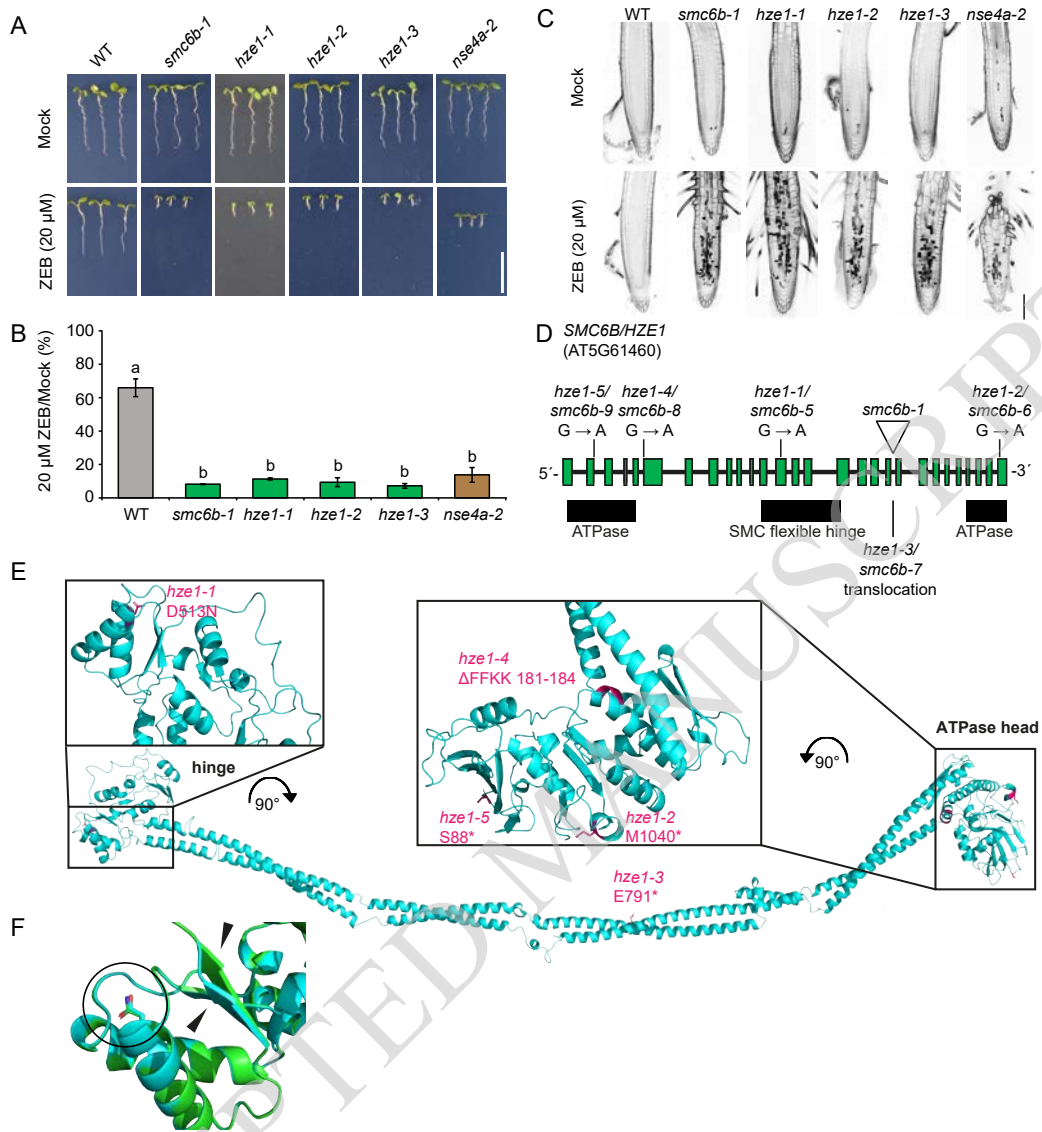
- 849 **Larsson, A.** (2014). AliView: A fast and lightweight alignment viewer and editor for large
850 datasets. *Bioinformatics* **30**: 3276–3278.
- 851 **Lee, J.H., Mosher, E.P., Lee, Y.S., Bumpus, N.N., and Berger, J.M.** (2022). Control of
852 topoisomerase II activity and chemotherapeutic inhibition by TCA cycle metabolites. *Cell*
853 *Chem Biol* **29**: 476-489.e6.
- 854 **Lee, J.H., Wendorff, T.J., and Berger, J.M.** (2017). Resveratrol: A novel type of
855 topoisomerase II inhibitor. *J Biol Chem* **292**: 21011–21022.
- 856 **Liu, C.-H.H., Finke, A., Díaz, M., Rozhon, W., Poppenberger, B., Baubec, T., and**
857 **Pecinka, A.** (2015). Repair of DNA damage induced by the cytidine analog zebularine
858 requires ATR and ATM in arabidopsis. *Plant Cell* **27**: 1788–1800.
- 859 **Liu, J.C.Y. et al.** (2021). Mechanism and function of DNA replication-independent DNA-
860 protein crosslink repair via the SUMO-RNF4 pathway. *EMBO J* **40**: e107413.
- 861 **Lobet, G., Pagès, L., and Draye, X.** (2011). A novel image-analysis toolbox enabling
862 quantitative analysis of root system architecture. *Plant Physiol* **157**: 29–39.
- 863 **Mannuss, A., Dukowic-Schulze, S., Suer, S., Hartung, F., Pacher, M., and Puchta, H.**
864 (2010). RAD5A, RECQ4A, AND MUS81 have specific functions in homologous
865 recombination and define different pathways of dna repair in *Arabidopsis thaliana*. *Plant*
866 *Cell* **22**: 3318–3330.
- 867 **Maslov, A.Y., Lee, M., Gundry, M., Gravina, S., Strogonova, N., Tazearslan, C.,**
868 **Bendebury, A., Suh, Y., and Vijg, J.** (2012). 5-Aza-2'-deoxycytidine-induced genome
869 rearrangements are mediated by DNMT1. *Oncogene* **31**: 5172–5179.
- 870 **Meneer, K.A. et al.** (2008). 4-[3-(4-Cyclopropanecarbonylpiperazine-1-carbonyl)-4-
871 fluorobenzyl]-2H-phthalazin-1-one: A novel bioavailable inhibitor of poly(ADP-ribose)
872 polymerase-1. *J. Med. Chem.* **51**: 6581–6591.
- 873 **Mengiste, T., Revenkova, E., Bechtold, N., and Paszkowski, J.** (1999). An SMC-like
874 protein is required for efficient homologous recombination in arabidopsis. *EMBO J* **18**:
875 4505–4512.
- 876 **Nakamura, J. and Nakamura, M.** (2020). DNA-protein crosslink formation by endogenous
877 aldehydes and AP sites. *DNA Repair (Amst)*. **88**: 102806.
- 878 **Nitiss, J.L. et al.** (2009). Targeting DNA topoisomerase II in cancer chemotherapy. *Nat Rev*
879 **9**: 338–350.
- 880 **Nowicka, A. et al.** (2020). Comparative analysis of epigenetic inhibitors reveals different
881 degrees of interference with transcriptional gene silencing and induction of DNA
882 damage. *Plant J* **102**: 68–84.
- 883 **Palecek, J.J.** (2019). SMC5/6: Multifunctional player in replication. *Genes (Basel)*. **10**.
- 884 **Pommier, Y. and Marchand, C.** (2012). Interfacial inhibitors: Targeting macromolecular
885 complexes. *Nat Rev Drug Discov* **11**: 25–36.

- 886 **Potts, P.R., Porteus, M.H., and Yu, H.** (2006). Human SMC5/6 complex promotes sister
887 chromatid homologous recombination by recruiting the SMC1/3 cohesin complex to
888 double-strand breaks. *EMBO J* **25**: 3377–3388.
- 889 **Pouliot, J.J., Yao, K.C., Robertson, C.A., and Nash, H.A.** (1999). Yeast gene for a Tyr-
890 DNA phosphodiesterase that repairs topoisomerase I complexes. *Science* **286**: 552–
891 555.
- 892 **Prochazkova, K., Finke, A., Dvořák Tomašíková, E., Filo, J., Bente, H., Dvořák, P.,**
893 **Ovečka, M., Šamaj, J., and Pecinka, A.** (2022). Zebularine induces enzymatic DNA–
894 protein crosslinks in 45S rDNA heterochromatin of *Arabidopsis* nuclei. *Nucleic Acids*
895 *Res* **50**: 244–258.
- 896 **Regairaz, M., Zhang, Y.W., Fu, H., Agama, K.K., Tata, N., Agrawal, S., Aladjem, M.I., and**
897 **Pommier, Y.** (2011). Mus81-mediated DNA cleavage resolves replication forks stalled
898 by topoisomerase I-DNA complexes. *J Cell Biol* **195**: 739–749.
- 899 **Reinking, H.K., Kang, H.S., Götz, M.J., Li, H.Y., Kieser, A., Zhao, S., Acampora, A.C.,**
900 **Weickert, P., Fessler, E., Jae, L.T., Sattler, M., and Stingele, J.** (2020). DNA
901 structure-specific cleavage of DNA-protein crosslinks by the SPRTN protease. *Mol Cell*
902 **80**: 102–113.
- 903 **Ruggiano, A., Vaz, B., Kilgas, S., Popović, M., Rodriguez-Berriguete, G., Singh, A.N.,**
904 **Higgins, G.S., Kiltie, A.E., and Ramadan, K.** (2021). The protease SPRTN and
905 SUMOylation coordinate DNA-protein crosslink repair to prevent genome instability. *Cell*
906 *Rep* **37**: 110080.
- 907 **Schellenberg, M.J., Lieberman, J.A., Herrero-Ruiz, A., Butler, L.R., Williams, J.G.,**
908 **Muñoz-Cabello, A.M., Mueller, G.A., London, R.E., Cortés-Ledesma, F., and**
909 **Williams, R.S.** (2017). ZATT (ZNF451)–mediated resolution of topoisomerase 2 DNA-
910 protein cross-links. *Science* **357**: 1412–1416.
- 911 **Schrödinger, LLC** (2015). The {PyMOL} Molecular Graphics System, Version~1.8.
- 912 **Serbyn, N., Bagdiul, I., Noireterre, A., Michel, A.H., Suhandynata, R.T., Zhou, H.,**
913 **Kornmann, B., and Stutz, F.** (2021). SUMO orchestrates multiple alternative DNA-
914 protein crosslink repair pathways. *Cell Rep* **37**: 110034.
- 915 **Stingele, J. et al.** (2016). Mechanism and regulation of DNA-protein crosslink repair by the
916 DNA-dependent metalloprotease SPRTN. *Mol Cell* **64**: 688–703.
- 917 **Stingele, J., Bellelli, R., and Boulton, S.J.** (2017). Mechanisms of DNA-protein crosslink
918 repair. *Nat Rev Mol Cell Biol* **18**: 563–573.
- 919 **Stingele, J. and Jentsch, S.** (2015). DNA-protein crosslink repair. *Nat Rev Mol Cell Biol* **16**:
920 455–460.
- 921 **Stingele, J., Schwarz, M.S., Bloemeke, N., Wolf, P.G., and Jentsch, S.** (2014). A DNA-
922 dependent protease involved in DNA-protein crosslink repair. *Cell* **158**: 327–338.

- 923 **Sun, Y., Jenkins, L.M.M., Su, Y.P., Nitiss, K.C., Nitiss, J.L., Pommier, Y., Miller Jenkins,**
 924 **L.M., Su, Y.P., Nitiss, K.C., Nitiss, J.L., and Pommier, Y.** (2020a). A conserved
 925 SUMO pathway repairs topoisomerase DNA-protein cross-links by engaging ubiquitin-
 926 mediated proteasomal degradation. *Sci Adv* **6**: eaba6290.
- 927 **Sun, Y., Saha, L.K., Saha, S., Jo, U., and Pommier, Y.** (2020b). Debulking of
 928 topoisomerase DNA-protein crosslinks (TOP-DPC) by the proteasome, non-
 929 proteasomal and non-proteolytic pathways. *DNA Repair (Amst)* **94**: 102926.
- 930 **Torres-Ramos, C.A., Prakash, S., and Prakash, L.** (2002). Requirement of RAD5 and
 931 MMS2 for Postreplication Repair of UV-Damaged DNA in *Saccharomyces cerevisiae*.
 932 *Mol Cell Biol* **22**: 2419–2426.
- 933 **Tsuda, M., Kitamasu, K., Kumagai, C., Sugiyama, K., Nakano, T., and Ide, H.** (2020).
 934 Tyrosyl-DNA phosphodiesterase 2 (TDP2) repairs topoisomerase 1 DNA-protein
 935 crosslinks and 3'-blocking lesions in the absence of tyrosyl-DNA phosphodiesterase 1
 936 (TDP1). *DNA Repair (Amst)* **91–92**: 102849.
- 937 **Varejão, N., Ibars, E., Lascorz, J., Colomina, N., Torres-Rosell, J., and Reverter, D.**
 938 (2018). DNA activates the Nse2/Mms21 SUMO E3 ligase in the Smc5/6 complex.
 939 *EMBO J* **37**: e98306 .
- 940 **Vaz, B. et al.** (2016). Metalloprotease SPRTN/DVC1 orchestrates replication-coupled DNA-
 941 protein crosslink repair. *Mol Cell* **64**: 704–719.
- 942 **Waldman, B.C. and Waldman, A.S.** (1990). Illegitimate and homologous recombination in
 943 mammalian cells: differential sensitivity to an inhibitor of poly(ADP-ribosylation). *Nucleic*
 944 *Acids Res* **18**: 5981–5988.
- 945 **Watanabe, K., Pacher, M., Dukowic, S., Schubert, V., Puchta, H., and Schubert, I.**
 946 (2009). The STRUCTURAL MAINTENANCE of CHROMOSOMES 5/6 complex
 947 promotes sister chromatid alignment and homologous recombination after DNA damage
 948 in *Arabidopsis thaliana*. *Plant Cell* **21**: 2688–2699.
- 949 **Waterhouse, A., Bertoni, M., Bienert, S., Studer, G., Tauriello, G., Gumienny, R., Heer,**
 950 **F.T., De Beer, T.A.P., Rempfer, C., Bordoli, L., Lepore, R., and Schwede, T.** (2018).
 951 SWISS-MODEL: homology modelling of protein structures and complexes. *Nucleic*
 952 *Acids Res.* **46**: W296–W303.
- 953 **Weickert, P. and Stingele, J.** (2022). DNA-Protein Crosslinks and Their Resolution. *Annu*
 954 *Rev Biochem* **91**: 157–181.
- 955 **Whalen, J.M., Dhingra, N., Wei, L., Zhao, X., and Freudenreich, C.H.** (2020). Relocation of
 956 Collapsed Forks to the Nuclear Pore Complex Depends on Sumoylation of DNA Repair
 957 Proteins and Permits Rad51 Association. *Cell Rep* **31**: 107635
- 958 **Willing, E.-M.M., Piofczyk, T., Albert, A., Winkler, J.B., Schneeberger, K., and Pecinka,**
 959 **A.** (2016). UVR2 ensures transgenerational genome stability under simulated natural

- 960 UV-B in *Arabidopsis thaliana*. *Nat Commun* **7**: 13522.
- 961 **Yang, F., Fernández Jiménez, N., Majka, J., Pradillo, M., and Pecinka, A.** (2021).
962 Structural Maintenance of Chromosomes 5/6 Complex Is Necessary for Tetraploid
963 Genome Stability in *Arabidopsis thaliana*. *Front Plant Sci* **12**: 748252.
- 964 **Yu, Y., Li, S., Ser, Z., Kuang, H., Than, T., Guan, D., Zhao, X., and Patel, D.J.** (2022).
965 Cryo-EM structure of DNA-bound Smc5/6 reveals DNA clamping enabled by multi-
966 subunit conformational changes. *Proc Natl Acad Sci U S A* **119**: e2202799119.
- 967 **Zhang, H., Xiong, Y., and Chen, J.** (2020). DNA–protein cross-link repair: what do we know
968 now? *Cell Biosci* **10**: 3..
- 969

ACCEPTED MANUSCRIPT

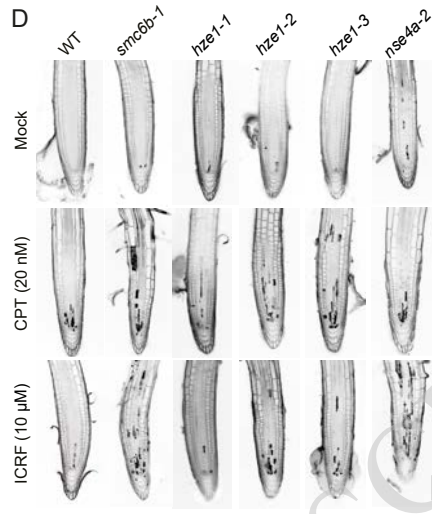
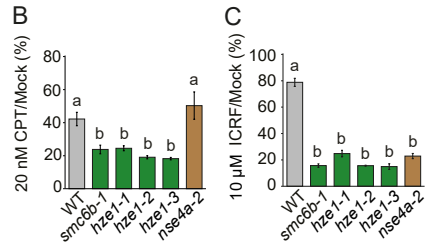
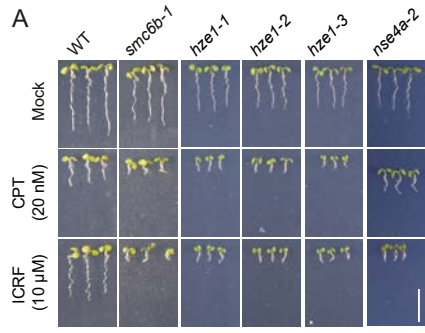


ACCEPTED MANUSCRIPT

Figure 1. *HYPERSENSITIVE TO ZEBULARINE 1 (HZE1)* encodes the SMC5/6 complex subunit SMC6B.

A, Representative growth phenotypes of seedlings from wild type (WT), *smc6b-1*, *hze1* alleles and *nse42-2* on 0 (Mock) and 20 μ M zebularine (ZEB). Scale bar, 1 cm. B, Relative root length of seedlings in (A) under zebularine/mock conditions (% of ZEB/Mock). Data are means \pm SD from three biological replicates, each with a minimum of 14 seedlings. Different lowercase letters indicate significant differences ($P < 0.05$), according to one-way ANOVA followed by Tukey's test. Source data for statistical analyses are available in Supplemental Table S1. The original experiment was split between Figures 1A-C, and Supplemental Figures S5A-D. Therefore, these figures show identical images and data for the controls. C, Representative confocal microscopy images of root tips stained with propidium iodide, which indicates dead cells (dark sectors). Five-day-old seedlings were treated with 20 μ M ZEB for 24 h prior to analysis. Scale bar, 100 μ m. D, Schematic model of the *SMC6B/HZE1* locus (At5g61460) with the positions of individual mutations. E, Detailed position of *hze1-1* to *hze1-5* mutations (magenta) in the AtSMC6B protein structure. The AtSMC6B (UniProt ACC: Q9FIIH) model was built using SWISS-MODEL using *Saccharomyces cerevisiae* SMC6 (PBDID: 7qcd) (Hallett et al., 2022) as template. F, Superposed models of the hinge domain from wild-type SMC6B (azure) and SMC6B in *hze1-1* (green) generated using AlphaFold2. Position of the D513N substitution is marked with black circle. The predicted effect on secondary structure is marked with black asterisks.

ACCEPTED MANUSCRIPT



ACCEPTED MANUSCRIPT

Figure 2. The SMC5/6 complex is required for the repair of type-3 and type-4 DNA protein crosslinks (DPCs).

A, Representative growth phenotype of wild-type (WT) and mutant seedlings on medium without DPC inducers (Mock) or containing 20 nM camptothecin (CPT) or 10 μ M ICRF-187 (ICRF). Scale bar, 1 cm. B, C, Relative root length of WT and mutant seedlings grown in the presence of 20 nM CPT (B) or 10 μ M ICRF (C). Data are means \pm SD from three biological replicates, each with at least 20 seedlings. Different letters indicate significant differences ($P < 0.05$) according to one-way ANOVA followed by Tukey's test. Source data for statistical analyses are available in Supplemental Table S2. The original experiment was split between Figure 2A-C and Supplemental Figures S5A-D. Therefore, these figures show identical images and data for the controls. D, Representative confocal microscopy images of root apices stained with propidium iodide. Five-day-old seedlings were treated for 24 h with 20 nM PT or 10 μ M ICRF prior to analysis. Dark sectors within the roots indicate dead cells. Scale bar, 100 μ m.

ACCEPTED MANUSCRIPT

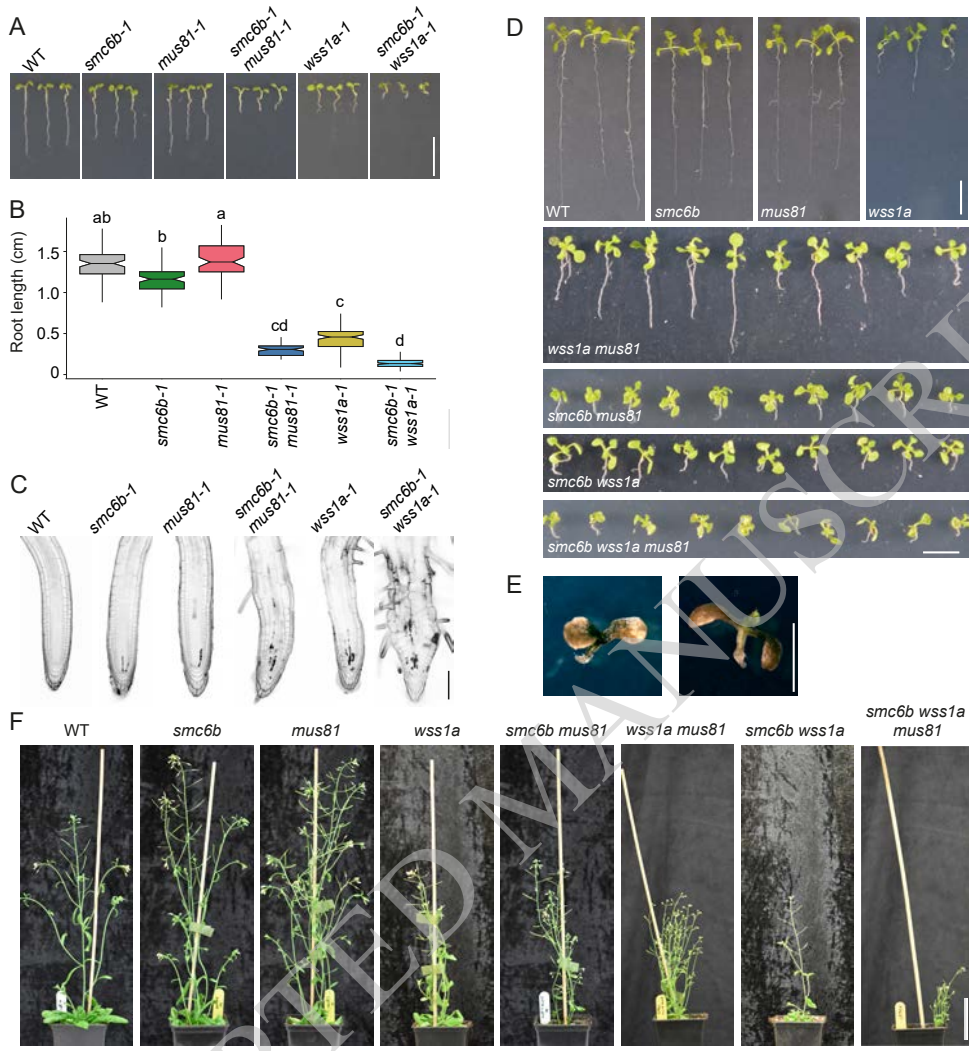
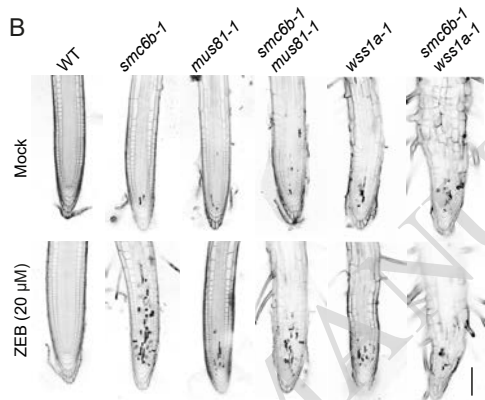
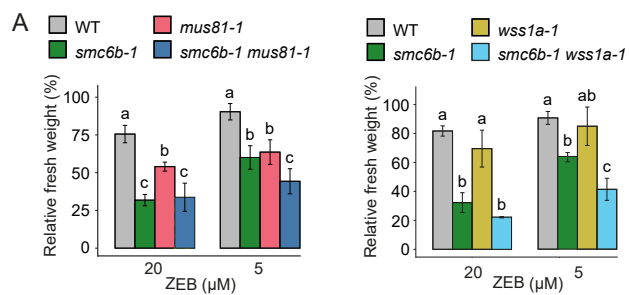


Figure 3. Phenotypic analysis of *smc6b-1*, *mus81-1*, *wss1a-1* and their higher-order mutants under normal conditions. A, Representative growth phenotype of wild type, *smc6b-1*, *mus81-1*, *wss1a-1* and double mutants with *smc6b-1*. Scale bar, 1 cm. B, Quantification of root length from A. At least 20 roots per genotype were analyzed in each of three biological replicates. The lower and upper hinges of the boxplots correspond to the first and third quartiles of the data, the black lines within the boxes indicates the median. Whiskers mark 10% and 90% intervals. Different letters indicate significant differences ($P < 0.05$) according to one-way ANOVA followed by Tukey's test. Source data for statistical analyses in B are available in Supplemental Table S4A. C, Representative confocal microscopy images of root tips stained with propidium iodide. Seedlings were grown for five days on control medium prior to analysis. Dark sectors indicate dead cells. Scale bar, 100 μm . D, Representative phenotypes of two-week-old WT, single mutants, double mutants, and *smc6b-1 mus81-1 wss1a-1* triple mutant seedlings grown on half-strength MS medium. Scale bar, 1 cm. E, Detailed photograph of three-week-old *smc6b-1 mus81-1 wss1a-1* triple mutant seedlings with severe phenotype grown on half-strength MS medium. Scale bar, 1 cm. F, Representative phenotypes of six-week old plants grown on soil. Scale bar, 70 mm.

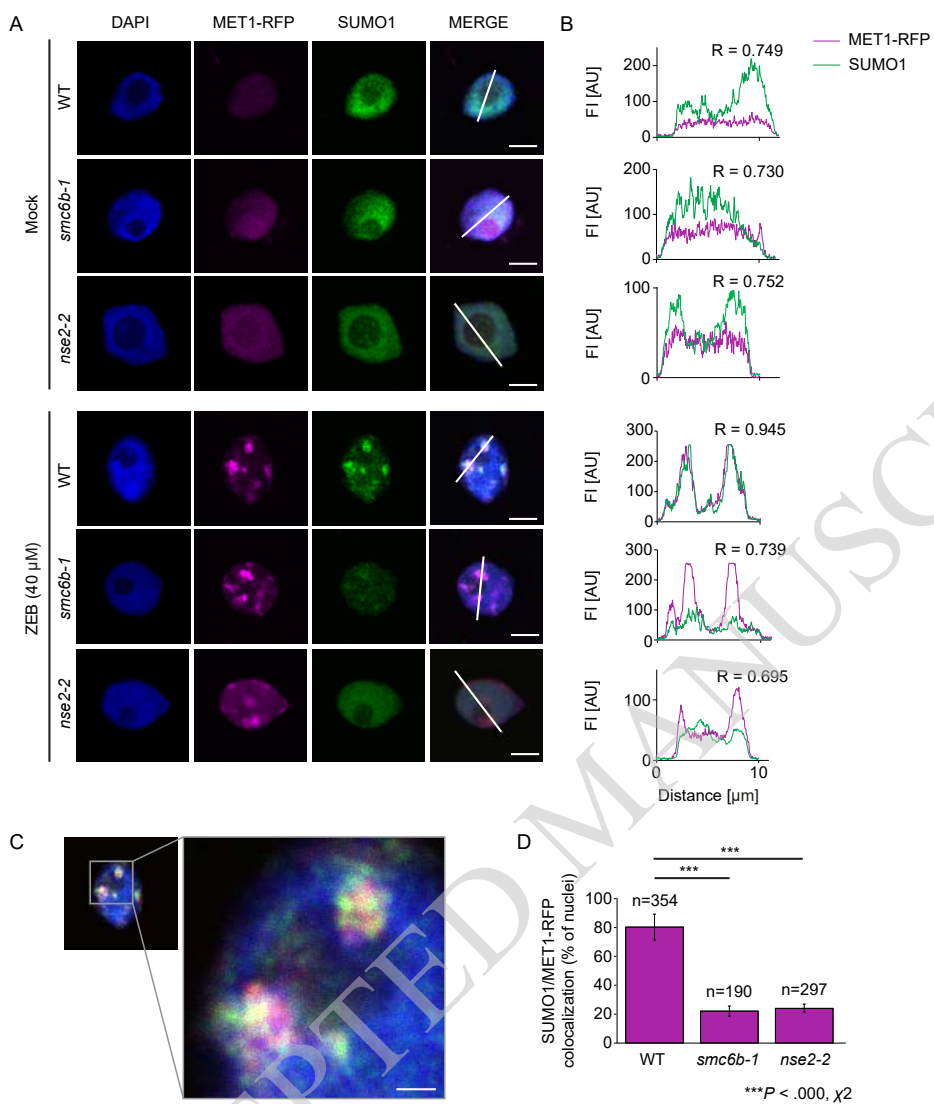
ACCEPTED MANUSCRIPT



ACCEPTED MANUSCRIPT

Figure 4. Sensitivity of *smc6b-1 mus81-1* and *smc6b-1 wss1a-1* plants to zebularine. A, Fresh weight of plants treated with 5 μ M or 20 μ M zebularine (ZEB). The sensitivity of double mutant plants was compared to the respective single mutants and WT plants relative to the mock-treated plants of the same genotype. Data are means \pm SD of three biological replicates. Different letters indicate significant differences ($P < 0.05$) according to one-way ANOVA followed by Tukey's test. Source data for A are available in Supplemental Table S4. B, Representative confocal microscopy images of root tips stained with propidium iodide. Scale bar, 100 μ m.

ACCEPTED MANUSCRIPT

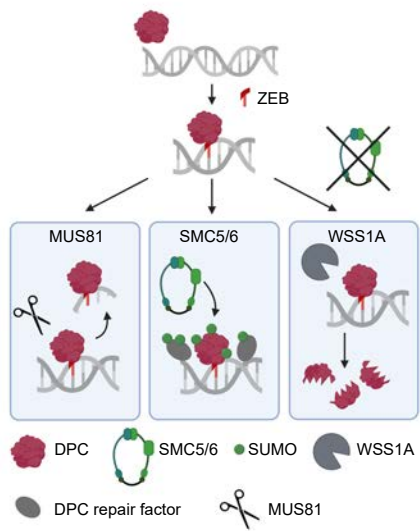


ACCEPTED MANUSCRIPT

Figure 5. SMC5/6-dependent SUMOylation of zebularine-induced MET1 crosslinks.

A, Immunolabeling of mock- and zebularine-treated WT, *smc6b-1*, and *nse2-2* root nuclei stained with SUMO1 antibody. MET1-RFP signals were observed directly, and nuclei were counterstained with DAPI. The white lines in Merge indicate intersects for fluorescence intensity measurements shown in (B). Scale bar, 5 μ m. B, Fluorescence intensity (FI) plots based on the white lines indicated intersects in (A). The y-axis shows FI intensity in arbitrary units (AU) for MET1-RFP and SUMO1 signals. R indicates Pearson's correlation coefficient assessment of colocalization (1, full colocalization). C, Detailed image of MET1-RFP colocalization with SUMO1 (from A) in WT nuclei after zebularine treatment. Scale bar, 1 μ m. D, Percentage of nuclei with MET1-RFP foci colocalizing with SUMO1 in WT, *smc6b-1* and *nse2-2* root nuclei after zebularine treatment. Data are means \pm SD from three biological replicates. Statistical significance was tested with chi-square test (*smc6b-1* χ^2 (2, N = 544) = 196.6331, p = .000, *nse2-2* (χ^2 (2, N = 651) = 231.7348, p = .000). n, total number of nuclei evaluated per genotype. Source data for the analyses are available in Supplemental Table S6.

ACCEPTED MANUSCRIPT



ACCEPTED MANUSCRIPT

Figure 6. Working model of zebularine-induced DPC repair. The endonuclease MUS81 cleaves DNA surrounding the crosslink. The SMC5/6 complex deposits SUMO residues on the MET1-DPC or adjacent repair proteins to stimulate repair. Without the SMC5/6 complex, the protease WSS1A proteolytically degrades the protein crosslinked by zebularine.

ACCEPTED MANUSCRIPT

Parsed Citations

- Alt, A, Dang, H.Q., Wells, O.S., Polo, L.M., Smith, M.A, McGregor, G.A, Welte, T., Lehmann, A.R., Pearl, L.H., Murray, J.M., and Oliver, A.W. (2017). Specialized interfaces of Smc5/6 control hinge stability and DNA association. *Nat Commun* 8, 14011.
Google Scholar: [Author Only](#) [Title Only](#) [Author and Title](#)
- Barker, S., Weinfeld, M., and Murray, D. (2005). DNA-protein crosslinks: their induction, repair, and biological consequences. *Mutat Res* 589: 111–135.
Google Scholar: [Author Only](#) [Title Only](#) [Author and Title](#)
- Bernges, F. and Zeller, W.J. (1996). Combination effects of poly(ADP-ribose) polymerase inhibitors and DNA-damaging agents in ovarian tumor cell lines--with special reference to cisplatin. *J Cancer Res Clin Oncol* 122: 665–670.
Google Scholar: [Author Only](#) [Title Only](#) [Author and Title](#)
- Bienert, S., Waterhouse, A, De Beer, T.A.P., Tauriello, G., Studer, G., Bordoli, L., and Schwede, T. (2017). The SWISS-MODEL Repository-new features and functionality. *Nucleic Acids Res* 45: D313–D319.
Google Scholar: [Author Only](#) [Title Only](#) [Author and Title](#)
- Borgermann, N., Ackermann, L., Schwertman, P., Hendriks, I.A, Thijssen, K., Liu, J.C., Lans, H., Nielsen, M.L., and Mailand, N. (2019). SUMOylation promotes protective responses to DNA-protein crosslinks. *EMBO J* 38: e101496.
Google Scholar: [Author Only](#) [Title Only](#) [Author and Title](#)
- Chen, X.B., Melchionna, R., Denis, C.M., Gaillard, P.H.L., Blasina, A, Van de Weyer, I., Boddy, M.N., Russell, P., Vialard, J., and McGowan, C.H. (2001). Human Mus81-associated endonuclease cleaves Holliday junctions in vitro. *Mol Cell* 8: 1117–1127.
Google Scholar: [Author Only](#) [Title Only](#) [Author and Title](#)
- Chen, Z, Yang, H., and Pavletich, N.P. (2008). Mechanism of homologous recombination from the RecA-ssDNA/dsDNA structures. *Nature* 453: 489–494.
Google Scholar: [Author Only](#) [Title Only](#) [Author and Title](#)
- Cingolani, P., Platts, A, Wang, L.L., Coon, M., Nguyen, T., Wang, L., Land, S.J., Lu, X., and Ruden, D.M. (2012). A program for annotating and predicting the effects of single nucleotide polymorphisms, SnpEff: SNPs in the genome of *Drosophila melanogaster* strain w1118; iso-2; iso-3. *Fly (Austin)*. 6: 80–92.
Google Scholar: [Author Only](#) [Title Only](#) [Author and Title](#)
- Classen, S., Olland, S., and Berger, J.M. (2003). Structure of the topoisomerase II ATPase region and its mechanism of inhibition by the chemotherapeutic agent ICRF-187. *Proc Natl Acad Sci U S A* 100: 10629–10634.
Google Scholar: [Author Only](#) [Title Only](#) [Author and Title](#)
- Core R Team (2020). A language and environment for statistical computing. *R Found. Stat. Comput.* 2: <https://www.R-project.org>.
Google Scholar: [Author Only](#) [Title Only](#) [Author and Title](#)
- Díaz, M. et al. (2019). The SMC5/6 complex subunit NSE4A is involved in DNA damage repair and seed development. *Plant Cell* 31: 1579–1597.
Google Scholar: [Author Only](#) [Title Only](#) [Author and Title](#)
- Diaz, M. and Pecinka, A (2018). Scaffolding for repair: understanding molecular functions of the SMC5/6 complex. *Genes (Basel)*. 9: 36.
Google Scholar: [Author Only](#) [Title Only](#) [Author and Title](#)
- Diaz, M., Pecinkova, P., Nowicka, A, Baroux, C., Sakamoto, T., Gandha, P.Y., Jeřábková, H., Matsunaga, S., Grossniklaus, U., and Pecinka, A. (2019). SMC5/6 Complex Subunit NSE4A is Involved in DNA Damage Repair and Seed Development in Arabidopsis. *Plant Cell* 31: 1579-1597. Doe, C.L., Ahn, J.S., Dixon, J., and Whitby, M.C. (2002). Mus81-Eme1 and Rqh1 involvement in processing stalled and collapsed replication forks. *J Biol Chem* 277: 32753–32759.
Google Scholar: [Author Only](#) [Title Only](#) [Author and Title](#)
- Dorn, A and Puchta, H. (2020). Analyzing somatic DNA repair in Arabidopsis meiotic mutants. *Methods Mol Biol* 2061: 359-366.
Google Scholar: [Author Only](#) [Title Only](#) [Author and Title](#)
- Enderle, J., Dorn, A, Beying, N., Trapp, O., and Puchta, H. (2019). The protease WSS1A, the endonuclease MUS81, and the phosphodiesterase TDP1 are involved in independent pathways of DNA-protein crosslink repair in plants. *Plant Cell* 31: 775–790.
Google Scholar: [Author Only](#) [Title Only](#) [Author and Title](#)
- Hacker, L. et al. (2020). Repair of DNA-protein crosslinks in plants. *DNA Repair (Amst)*. 87: 102787.
Google Scholar: [Author Only](#) [Title Only](#) [Author and Title](#)
- Hacker, L., Dorn, A, Enderle, J., and Puchta, H. (2022). The repair of topoisomerase 2 cleavage complexes in Arabidopsis. *Plant Cell* 34: 287–301.
Google Scholar: [Author Only](#) [Title Only](#) [Author and Title](#)

recombination in arabidopsis. *EMBO J* 18: 4505–4512.

Google Scholar: [Author Only](#) [Title Only](#) [Author and Title](#)

Nakamura, J. and Nakamura, M. (2020). DNA-protein crosslink formation by endogenous aldehydes and AP sites. *DNA Repair (Amst)*. 88: 102806.

Google Scholar: [Author Only](#) [Title Only](#) [Author and Title](#)

Nitiss, J.L. et al. (2009). Targeting DNA topoisomerase II in cancer chemotherapy. *Nat Rev* 9: 338–350.

Google Scholar: [Author Only](#) [Title Only](#) [Author and Title](#)

Nowicka, A et al. (2020). Comparative analysis of epigenetic inhibitors reveals different degrees of interference with transcriptional gene silencing and induction of DNA damage. *Plant J* 102: 68–84.

Google Scholar: [Author Only](#) [Title Only](#) [Author and Title](#)

Palecek, J.J. (2019). SMC5/6: Multifunctional player in replication. *Genes (Basel)*. 10.

Google Scholar: [Author Only](#) [Title Only](#) [Author and Title](#)

Pommier, Y. and Marchand, C. (2012). Interfacial inhibitors: Targeting macromolecular complexes. *Nat Rev Drug Discov* 11: 25–36.

Google Scholar: [Author Only](#) [Title Only](#) [Author and Title](#)

Potts, P.R., Porteus, M.H., and Yu, H. (2006). Human SMC5/6 complex promotes sister chromatid homologous recombination by recruiting the SMC1/3 cohesin complex to double-strand breaks. *EMBO J* 25: 3377–3388.

Google Scholar: [Author Only](#) [Title Only](#) [Author and Title](#)

Pouliot, J.J., Yao, K.C., Robertson, C.A., and Nash, H.A. (1999). Yeast gene for a Tyr-DNA phosphodiesterase that repairs topoisomerase I complexes. *Science* 286: 552–555.

Google Scholar: [Author Only](#) [Title Only](#) [Author and Title](#)

Prochazkova, K., Finke, A., Dvořák Tomašíková, E., Filo, J., Bente, H., Dvořák, P., Ovečka, M., Šamaj, J., and Pecinka, A. (2022). Zebularine induces enzymatic DNA-protein crosslinks in 45S rDNA heterochromatin of Arabidopsis nuclei. *Nucleic Acids Res* 50: 244–258.

Google Scholar: [Author Only](#) [Title Only](#) [Author and Title](#)

Regairaz, M., Zhang, Y.W., Fu, H., Agama, K.K., Tata, N., Agrawal, S., Aladjem, M.I., and Pommier, Y. (2011). Mus81-mediated DNA cleavage resolves replication forks stalled by topoisomerase I-DNA complexes. *J Cell Biol* 195: 739–749.

Google Scholar: [Author Only](#) [Title Only](#) [Author and Title](#)

Reinking, H.K., Kang, H.S., Götz, M.J., Li, H.Y., Kieser, A., Zhao, S., Acampora, A.C., Weickert, P., Fessler, E., Jae, L.T., Sattler, M., and Stinglele, J. (2020). DNA structure-specific cleavage of DNA-protein crosslinks by the SPRTN protease. *Mol Cell* 80: 102–113.

Google Scholar: [Author Only](#) [Title Only](#) [Author and Title](#)

Ruggiano, A, Vaz, B., Kilgas, S., Popović, M., Rodriguez-Berriguete, G., Singh, A.N., Higgins, G.S., Kiltie, A.E., and Ramadan, K. (2021). The protease SPRTN and SUMOylation coordinate DNA-protein crosslink repair to prevent genome instability. *Cell Rep* 37: 110080.

Google Scholar: [Author Only](#) [Title Only](#) [Author and Title](#)

Schellenberg, M.J., Lieberman, J.A., Herrero-Ruiz, A., Butler, L.R., Williams, J.G., Muñoz-Cabello, A.M., Mueller, G.A., London, R.E., Cortés-Ledesma, F., and Williams, R.S. (2017). ZATT (ZNF451)-mediated resolution of topoisomerase 2 DNA-protein crosslinks. *Science* 357: 1412–1416.

Google Scholar: [Author Only](#) [Title Only](#) [Author and Title](#)

Schrödinger, LLC (2015). The {PyMOL} Molecular Graphics System, Version~1.8.

Serbyn, N., Bagdiul, I., Noireterre, A., Michel, A.H., Suhandynata, R.T., Zhou, H., Kornmann, B., and Stutz, F. (2021). SUMO orchestrates multiple alternative DNA-protein crosslink repair pathways. *Cell Rep* 37: 110034.

Google Scholar: [Author Only](#) [Title Only](#) [Author and Title](#)

Stinglele, J. et al. (2016). Mechanism and regulation of DNA-protein crosslink repair by the DNA-dependent metalloprotease SPRTN. *Mol Cell* 64: 688–703.

Google Scholar: [Author Only](#) [Title Only](#) [Author and Title](#)

Stinglele, J., Bellelli, R., and Boulton, S.J. (2017). Mechanisms of DNA-protein crosslink repair. *Nat Rev Mol Cell Biol* 18: 563–573.

Google Scholar: [Author Only](#) [Title Only](#) [Author and Title](#)

Stinglele, J. and Jentsch, S. (2015). DNA-protein crosslink repair. *Nat Rev Mol Cell Biol* 16: 455–460.

Google Scholar: [Author Only](#) [Title Only](#) [Author and Title](#)

Stinglele, J., Schwarz, M.S., Bloemke, N., Wolf, P.G., and Jentsch, S. (2014). A DNA-dependent protease involved in DNA-protein crosslink repair. *Cell* 158: 327–338.

Google Scholar: [Author Only](#) [Title Only](#) [Author and Title](#)

- Sun, Y., Jenkins, L.M.M., Su, Y.P., Nitiss, K.C., Nitiss, J.L., Pommier, Y., Miller Jenkins, L.M., Su, Y.P., Nitiss, K.C., Nitiss, J.L., and Pommier, Y. (2020a). A conserved SUMO pathway repairs topoisomerase DNA-protein cross-links by engaging ubiquitin-mediated proteasomal degradation. *Sci Adv* 6: eaba6290.
Google Scholar: [Author Only](#) [Title Only](#) [Author and Title](#)
- Sun, Y., Saha, L.K., Saha, S., Jo, U., and Pommier, Y. (2020b). Debulking of topoisomerase DNA-protein crosslinks (TOP-DPC) by the proteasome, non-proteasomal and non-proteolytic pathways. *DNA Repair (Amst)* 94: 102926.
Google Scholar: [Author Only](#) [Title Only](#) [Author and Title](#)
- Torres-Ramos, C.A., Prakash, S., and Prakash, L. (2002). Requirement of RAD5 and MMS2 for Postreplication Repair of UV-Damaged DNA in *Saccharomyces cerevisiae*. *Mol Cell Biol* 22: 2419–2426.
Google Scholar: [Author Only](#) [Title Only](#) [Author and Title](#)
- Tsuda, M., Kitamasu, K., Kumagai, C., Sugiyama, K., Nakano, T., and Ide, H. (2020). Tyrosyl-DNA phosphodiesterase 2 (TDP2) repairs topoisomerase 1 DNA-protein crosslinks and 3'-blocking lesions in the absence of tyrosyl-DNA phosphodiesterase 1 (TDP1). *DNA Repair (Amst)* 91–92: 102849.
Google Scholar: [Author Only](#) [Title Only](#) [Author and Title](#)
- Varejão, N., Ibars, E., Lascorz, J., Colomina, N., Torres-Rosell, J., and Reverter, D. (2018). DNA activates the Nse2/Mms21 SUMO E3 ligase in the Smc5/6 complex. *EMBO J* 37: e98306 .
Google Scholar: [Author Only](#) [Title Only](#) [Author and Title](#)
- Vaz, B. et al. (2016). Metalloprotease SPRTN/DVC1 orchestrates replication-coupled DNA-protein crosslink repair. *Mol Cell* 64: 704–719.
Google Scholar: [Author Only](#) [Title Only](#) [Author and Title](#)
- Waldman, B.C. and Waldman, A.S. (1990). Illegitimate and homologous recombination in mammalian cells: differential sensitivity to an inhibitor of poly(ADP-ribosylation). *Nucleic Acids Res* 18: 5981–5988.
Google Scholar: [Author Only](#) [Title Only](#) [Author and Title](#)
- Watanabe, K., Pacher, M., Dukowic, S., Schubert, V., Puchta, H., and Schubert, I. (2009). The STRUCTURAL MAINTENANCE OF CHROMOSOMES 5/6 complex promotes sister chromatid alignment and homologous recombination after DNA damage in *Arabidopsis thaliana*. *Plant Cell* 21: 2688–2699.
Google Scholar: [Author Only](#) [Title Only](#) [Author and Title](#)
- Waterhouse, A., Bertoni, M., Bienert, S., Studer, G., Tauriello, G., Gumienny, R., Heer, F.T., De Beer, T.A.P., Rempfer, C., Bordoli, L., Lepore, R., and Schwede, T. (2018). SWISS-MODEL: homology modelling of protein structures and complexes. *Nucleic Acids Res.* 46: W296–W303.
Google Scholar: [Author Only](#) [Title Only](#) [Author and Title](#)
- Weickert, P. and Stingle, J. (2022). DNA-Protein Crosslinks and Their Resolution. *Annu Rev Biochem* 91: 157–181.
Google Scholar: [Author Only](#) [Title Only](#) [Author and Title](#)
- Whalen, J.M., Dhingra, N., Wei, L., Zhao, X., and Freudenreich, C.H. (2020). Relocation of Collapsed Forks to the Nuclear Pore Complex Depends on Sumoylation of DNA Repair Proteins and Permits Rad51 Association. *Cell Rep* 31: 107635
Google Scholar: [Author Only](#) [Title Only](#) [Author and Title](#)
- Willing, E.-M.M., Piofczyk, T., Albert, A., Winkler, J.B., Schneeberger, K., and Pecinka, A. (2016). UVR2 ensures transgenerational genome stability under simulated natural UV-B in *Arabidopsis thaliana*. *Nat Commun* 7: 13522.
Google Scholar: [Author Only](#) [Title Only](#) [Author and Title](#)
- Yang, F., Fernández Jiménez, N., Majka, J., Pradillo, M., and Pecinka, A. (2021). Structural Maintenance of Chromosomes 5/6 Complex Is Necessary for Tetraploid Genome Stability in *Arabidopsis thaliana*. *Front Plant Sci* 12: 748252.
Google Scholar: [Author Only](#) [Title Only](#) [Author and Title](#)
- Yu, Y., Li, S., Ser, Z., Kuang, H., Than, T., Guan, D., Zhao, X., and Patel, D.J. (2022). Cryo-EM structure of DNA-bound Smc5/6 reveals DNA clamping enabled by multi-subunit conformational changes. *Proc Natl Acad Sci U S A* 119: e2202799119.
Google Scholar: [Author Only](#) [Title Only](#) [Author and Title](#)
- Zhang, H., Xiong, Y., and Chen, J. (2020). DNA-protein cross-link repair: what do we know now? *Cell Biosci* 10: 3.
Google Scholar: [Author Only](#) [Title Only](#) [Author and Title](#)